A Review and Application of the Hadron Gas Model to Heavy Ion Collisions

Duncan Mark Elliott

April 17, 1996

Abstract

A review and application of the Hadron Gas model to data gathered from heavy ion collision experiments in search of the Quark Gluon Plasma. The Hadron Gas model is extended by ensuring overall charge conservation of the collision system at freeze-out. Conclusions of thermal and chemical equilibrium at freeze-out are drawn from an analysis of the data of $Si - Au$ collisions at BNL-AGS, and compared with the literature on thermal analyses of $Si - Au$ collisions.

Contents

List of Figures

List of Tables

Chapter 1

The Search for the Quark Gluon Plasma

1.1 Introduction.

The goal of ultra-relativistic heavy ion physics is to study hadronic matter under extreme densities and temperatures, in a search for evidence of the Quark Gluon Plasma (QGP). Lattice QCD predicted a phase transition from the hadronic to a plasma state, where the quarks and gluons are free to move over a large volume compared with the typical size of hadrons [1]. Under very similar conditions that lead to this 'deconfinement' of the quarks, chiral symmetry restoration, which sees the quark massses drop to zero, is also predicted to occur. The order of the phase transition to a QGP is of great interest, but it is still unclear whether the transition is of first or second order.

The promise of 'new' physics galvanized physicists into designing experiments that could provide the densities and temperatures predicted for the phase change to a QGP, especially at the AGS in Brookhaven National Laboratory and SPS at CERN. A first round of ultra-relativistic light ions (O, Si, S) has been completed in the above laboratories and the energy densities reached are comparable with those predicted for the phase transition to occur [2]. Much experience has been gained in handling the experimental difficulties involved in collisions with so many events, and appropriate experimental tools have been developed.

A second round of heavy ion collisions has now begun, with 10 GeV/u $Au - Au$ collisions at the AGS (1992), and 160 GeV/u $Pb - Pb$ collisions at CERN (1994). These collisions provide a considerable increase in the volume of the system, but only a slight increase in energy density [3].

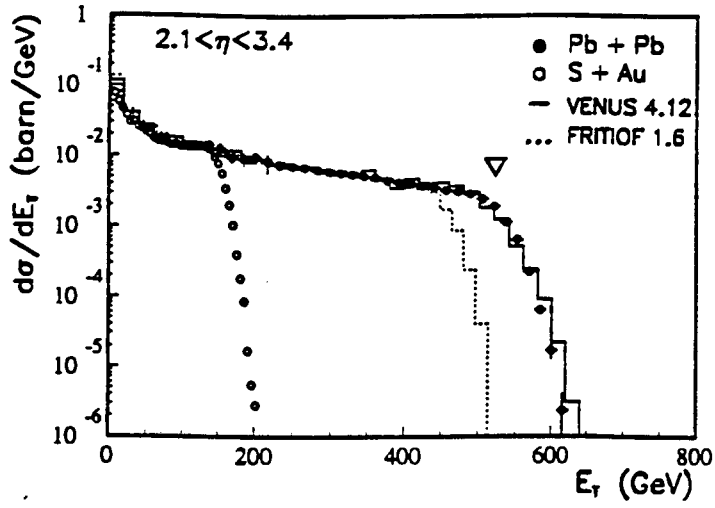

Figure 1.1: Transverse energy distribution of $Pb - Pb$ at 160 GeV/A and $S - Au$ at 200 GeV/A compared with calculations using the FRITIOF and VENUS event generators [6].

1.2 Global and hadronic observables.

Observables like the total transverse energy of the collision system, E_T, and the charged particle distribution are termed 'global' observables, whilst 'hadronic' observables include p_T spectra and particle production cross sections. They provide information about the system or 'fireball' at freeze-out (i.e. when the hadrons cease to interact).
If the QGP is attained in these collisions physicists require experimental evidence for its existence i.e. signatures of the QGP. Quite a number of signatures have been proposed. However, in a later section of this chapter, I will only briefly review the signature which pertains to the Hadron Gas model: strangeness enhancement [4].

1.3 Thermal and chemical equilibrium.

Does the system reach thermal and chemical equilibrium to justify the use of statistical QCD and thermodynamics as the appropriate theoretical framework in describing these collisions? Is there sufficient scattering and rescattering of the incident and produced particles that thermalisation occurs (i.e. all particles in the fireball share the same temperature)?
Comparing the measured transverse energy, E_T, with event generators (with, and without scattering) it seems that a large degree of scattering and rescattering does indeed take place [5]. The energy density, ϵ, is inferred from the energy deposited in the system - reflected in the measured transverse energy (or number of particles produced) - *together* with a model of the initial interaction volume. The boost-invariant Bjorken model [7] is the most popular

model, where the energy density, ϵ, is given by

$$\epsilon = 1/(\pi R^2 \tau) \frac{dE_T}{dy} , \tag{1.1}$$

where R is the projectile radius ($R = 1.12A^{1/3}$), and τ is the formation time (usually assumed to be $\sim$ 1 fm/c). The energy densities achieved at SPS are 3.2 GeV/fm^3 ($Pb-Pb$ at 160 GeV/A) and 2.6 GeV/fm^3 ($S-Au$ at 200 GeV/A) [6]. These values are about 20 times larger than normal nuclear matter ($\sim$ 0.16 GeV/fm^3) and about 7 times larger than inside a nucleon. More importantly, these values are within the range of values predicted for the deconfinement phase transition to occur.

Testing the thermal hypothesis requires detailed study of the particle abundances over the whole phase space. Assuming an ideal gas (of quarks and antiquarks in the QGP phase, and hadrons and hadronic resonances in the hadronic phase) is produced in chemical equilibrium, then *all* particle production ratios are specified by two independent variables: temperature, T, and baryon chemical potential, μ_B.

There are claims that both thermal and chemical equilibrium have been reached at AGS and SPS energies [29, 8] . Although there is remarkable agreement of the data with a thermal analysis, there are some problems with such an approach. A review of the thermal, or Hadron Gas model, follows in Chapter 2.

1.4 A first attempt at modelling the equation of state of the QGP phase.

In order to investigate the properties of the QGP, and its possible formation, we have to derive its equation of state. Assuming thermalisation (which was necessary to create the plasma in the first place), using massless quarks and gluons and neglecting interactions among them, we can make a first semi-quantitative attempt at some insight into a QGP [9].

Looking at the degrees of freedom in each constituent of the plasma, we have 16 for the gluons (2 spin $\times$ 8 colour) and 12 for the quarks (2 spin $\times$ 3 colour $\times$ 2 flavour). Now we can calculate the energy density residing in each degree of freedom.

An ideal relativistic Bose gas of gluons, without interactions, using $\beta = T^{-1}$ is given by

$$\epsilon_g = \int \frac{d^3p}{(2\pi)^3} p^3 (e^{\beta p} - 1)^{-1}. \tag{1.2}$$

Rescaling p, and making use of

$$\int_0^\infty dx x^{n-1}(e^x - 1)^{-1} = \Gamma(n)\zeta(n) = \pi^4/15 \quad (n = 4), \tag{1.3}$$

gives the result:

$$\epsilon_g = \pi^2 T^4/30. \tag{1.4}$$

For the quarks and antiquarks a chemical potential has to be introduced as there will in general be a surplus of quarks over antiquarks in the QGP, since nuclear collisions carry a net baryon number which is conserved. The energy density residing in the quarks alone, or the antiquarks alone, cannot be calculated analytically, but, fortunately, the sum of both the quark and antiquark energy density yields a simple analytical formula. An ideal relativistic Fermi gas of massless quarks and antiquarks ($E = p$), without interactions, using $\beta = T^{-1}$ is given by

$$\epsilon_q + \epsilon_{\bar{q}} = \int \frac{d^3p}{(2\pi)^3} p(e^{\beta(p-\mu)} + 1)^{-1} + \int \frac{d^3p}{(2\pi)^3} p(e^{\beta(p+\mu)} + 1)^{-1} \tag{1.5}$$

which after some manipulation (see Appendix A for a similar calculation) results in

$$\epsilon_q + \epsilon_{\bar{q}} = 7\pi^2 T^4/120 + \mu^2 T^2/4 + \mu^4/8\pi^2. \tag{1.6}$$

Now, in order to get an indication of the range of energy densities involved in QGP physics, we can find the total energy density in a baryon number-symmetric quark-gluon gas. This entails multiplying eq.(1.4) and eq.(1.6) by the number of respective degrees of freedom,

$$\epsilon_{\mathrm{QGP}} = 16\epsilon_g + 12(\epsilon_q + \epsilon_{\bar{q}}) = 37\pi^2 T^4/30 = (T/160\mathrm{MeV})^4 \ \mathrm{GeV/fm^3}. \tag{1.7}$$

Comparing this result with the energy density in nuclear matter, $\epsilon_{nuc} \simeq 125$ MeV/fm^3 and the energy density inside a nucleon which is four times the MIT-bag constant $\epsilon_{n,p} \simeq 4\mathrm{B} \simeq$ 300-500 MeV/fm^3. Since the critical temperature, T_c, is predicted to be 150 ± 50 MeV, we conclude, within the MIT-bag model approach, that the energy density in the QGP must be at least double the energy density inside a nucleon.

The baryon density, n_B is one third of the difference between the density of quarks (n_q) and the density of antiquarks ($n_{\bar{q}}$). As above, per degree of freedom:

$$n_q = \int \frac{d^3p}{(2\pi)^3} (e^{\beta(p-\mu)} + 1)^{-1} \tag{1.8}$$

and

$$n_{\bar{q}} = \int \frac{d^3p}{(2\pi)^3} (e^{\beta(p+\mu)} + 1)^{-1}. \tag{1.9}$$

The full calculation of $n_q - n_{\bar{q}}$ is given in Appendix A. Quoting the result of this calculation

$$n_q - n_{\bar{q}} = [\mu T^2 + \mu^3/\pi^2]/6 \tag{1.10}$$

we can calculate n_B

$$n_B = 12[n_q - n_{\bar{q}}]/3 = 2\mu T^2/3 + 2\mu^3/3\pi^2. \tag{1.11}$$

Again, we find the relation

$$n_B = 4/3\frac{\partial \epsilon}{\partial \mu} \tag{1.12}$$

which has a fundamental thermodynamic origin.

In a first attempt to compare the energy densities of the hadronic phase with the QGP phase, we can calculate the energy density of a 'free' pion gas (massless, non-interacting pions) by multiplying eq.(1.4) by the degrees of freedom of pions, i.e.

$$\epsilon_\pi = 3\pi^2 T^4/30. \tag{1.13}$$

Comparing the result for ϵ_{QGP} in eq.(1.7) with the result for ϵ_π, we see that both energy densities grow as T^4, but the coefficients are an order of magnitude different. At the critical temperature, T_c, the pion gas undergoes a phase transition, and the now deconfined quarks are described by a different equation of state, a state with much greater energy density.

1.5 Signatures of the QGP.

Numerous signatures of a Quark Gluon Plasma have been proposed. Strangeness enhancement was one of the first [4]. Briefly, the mechanism for this enhancement is the decrease of the strange quark mass in the plasma, combined with the large chemical potential for u and d quarks due to the large number of valence quarks, which all favour the production of $s\bar{s}$ pairs. Experiments have shown that there is enhancement of strange particles, particularly strange and multistrange antibaryons [10, 29, 53]. However, there are reservations as to whether this phenomenon is due to the mechanism outlined above. Further discussion in this regard is found in Chapter 4.

There has also been experimental evidence in support of other proposed signatures of the QGP. J/Ψ suppression, proposed by [11], has been seen [12], and very exciting results have been found [13] with regard to the dilepton pairs signature proposed by [14].

There seems to be mounting evidence that a Quark Gluon Plasma phase is indeed attainable in the laboratory. However, not everyone is convinced for the need to invoke a new phase of matter to explain the data. Perhaps the new round of experiments at SPS and the AGS will resolve this question?

Chapter 2

Hadron Gas model

2.1 Introduction.

The Hadron Gas model seeks to describe the resulting fireball and its freeze-out hadronic constituents in a thermal, chemically equilibrated manner, where each hadronic species is represented by its statistical weight.

The (invariant) momentum spectrum of a locally thermalised emitter is given by the Cooper-Frye formula [15],

$$E\frac{d^3N_i}{d^3p} = \frac{1}{(2\pi)^3}\int_{\Sigma_f} f_i(x,p)p^\mu d^3\Sigma_\mu(x), \tag{2.1}$$

with $f_i(x,p)$ the phase space distribution, and Σ_f a three dimensional freeze-out hypersurface (spherical in the stationary fireball case). In a stationary, equilibrated fireball the phase space distribution function $f(x,p)$ does not depend on x: in the Boltzmann approximation we have

$$f_i(x,p) = \lambda_i e^{(-p^\mu u_\mu/T)}, \tag{2.2}$$

where $\lambda_i = e^{(\mu_i/T)}$ is the fugacity and

$$u^\mu = (\cosh y_{FB}, 0, 0, \sinh y_{FB}) \tag{2.3}$$

is the constant 4-velocity of the fireball centre of mass frame relative to the observer frame, and

$$p^\mu = (m_T \cosh y, 0, 0, m_T \sinh y) \tag{2.4}$$

is the 4-momentum of the beam. If at freeze-out we have an ideal gas of hadrons and hadronic resonances, then the system is described by the partition function

$$\ln Z(T, \mu_B, \mu_S, \mu_Q) = \sum_i \lambda^i W_i. \tag{2.5}$$

Here W_i is the phase space factor for hadrons of species i. The phase space factors are given by

$$W_i = \frac{g_i m_i^2 VT}{2\pi^2} K_2\left(\frac{m_i}{T}\right), \tag{2.6}$$

with g_i denoting the spin degeneracy, m_i the mass of hadron species i; V is the volume of the system.

In the derivation of equation (2.6), it proves advantageous to transform from Cartesian coordinates to cylindrical coordinates, which describe the collision far more intuitively. A full treatment of the transformation to cylindrical coordinates, and the derivation of equation (2.6) is given in Appendices B and C.

2.2 Cylindrical symmetry.

Due to the cylindrical symmetry of the collision it is convenient to introduce two variables: longitudinal rapidity, y, and transverse mass, m_T.

The rapidity, y, is defined as

$$y = \tanh^{-1}\left(\frac{p_z}{E}\right), \tag{2.7}$$

and m_T as

$$m_T = \sqrt{m^2 + p_x^2 + p_y^2}. \tag{2.8}$$

The Boltzmann distribution function predicts for hadron species i a particle density

$$N_i = g_i \lambda_i V \int \frac{d^3p}{(2\pi)^3}\, e^{\frac{-E_i}{T}}\ . \tag{2.9}$$

The transformation to cylindrical coordinates allows us to rephrase eq.(2.9) (see Appendix D for a fuller treatment) as

$$n_i = \frac{N_i}{V} = \frac{g_i}{(2\pi)^2}\ e^{\frac{\mu_i}{T}} \int_0^\infty dy \int_m^\infty dm_T m_T E e^{\frac{-m_T}{T}} \cosh y, \tag{2.10}$$

which is rewritten in the form

$$\frac{dn_i}{m_T{}^2 dm_T} = \frac{g_i}{(2\pi)^2}\ e^{\frac{\mu_i}{T}}\ K_1\left(\frac{m_T}{T}\right). \tag{2.11}$$

If we investigate the behaviour of the K_1 function when its argument becomes large we see that $\lim_{z\to\infty} K_1(z) = \sqrt{\frac{\pi}{2z}}\ \ e^{-z}$. Finally, substituting $z = \left(\frac{m_T}{T}\right)$ we reach

$$\lim_{(m_T/T)\to\infty} \frac{dn_i}{dm_T} \propto m_T^{\frac{3}{2}}\, e^{\left(\frac{-m_T}{T}\right)}. \tag{2.12}$$

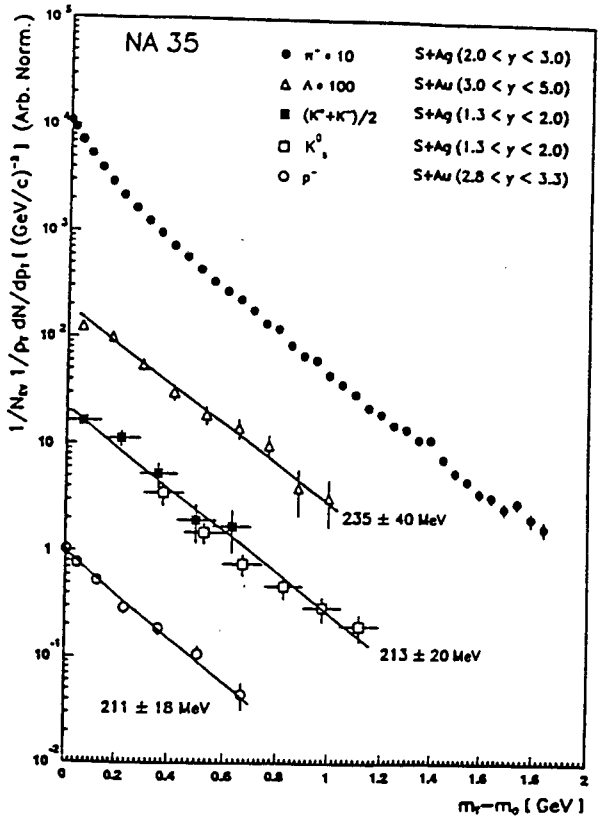

Figure 2.1: m_T scaling: Plots of $1/p_T dN/dp_T$ as a function of $m_T - m_0$ (arb. normalisation). Note π^- low p_T anomaly [16]. Note $1/p_T dN/dp_T$ is plotted due to small rapidity intervals (see App. E).

2.3 m_T scaling.

Looking at equation (2.12), logarithmic plots of $dn_i/(m_T^{\frac{3}{2}} dm_T)$ vs m_T should belie the Boltzmann behaviour. All particles from a thermalised emitter should show the the same universal exponential behaviour in their m_T spectra - m_T scaling.

It is very encouraging indeed to see the slope (i.e. T^{-1}) consistent over several orders of magnitude. Note: When the rapidity window of the collected data is small, we should not plot $dn/(m_T^{\frac{3}{2}}\, dm_T)$ vs m_T, but rather $dn/(dy dm_T)$ vs m_T, which behaves as $e^{\frac{-m_T}{T_{\rm eff}}}$ with $T_{\rm eff} = T/\cosh(y - y_{FB})$. See Appendix E in this regard.

An even more illuminating plot is a plot of $dn_i/(m_T^{\frac{3}{2}} dm_T)$ vs $m_T - m_0$, and once again the thermal nature is well shown, except for the pions which show a concave curvature, so a single thermal source cannot fit both the low and the high m_T region. The pions have a steeper tail at low p_T, indicating a lower characteristic 'temperature'. This phenomenon has been accounted for phenomenologically by including pions of resonance decay origin, which severely contaminate the thermal slope of the pion spectrum. This a very plausible argument as we see that the decay pions rapidly outgrow the thermal pions at typical values of temperature and baryonic density for $Si - Au$ experiments at the AGS (see Fig.(4.2)). Arguing that these decay pions don't have time to thermalise they steepen the slope at low

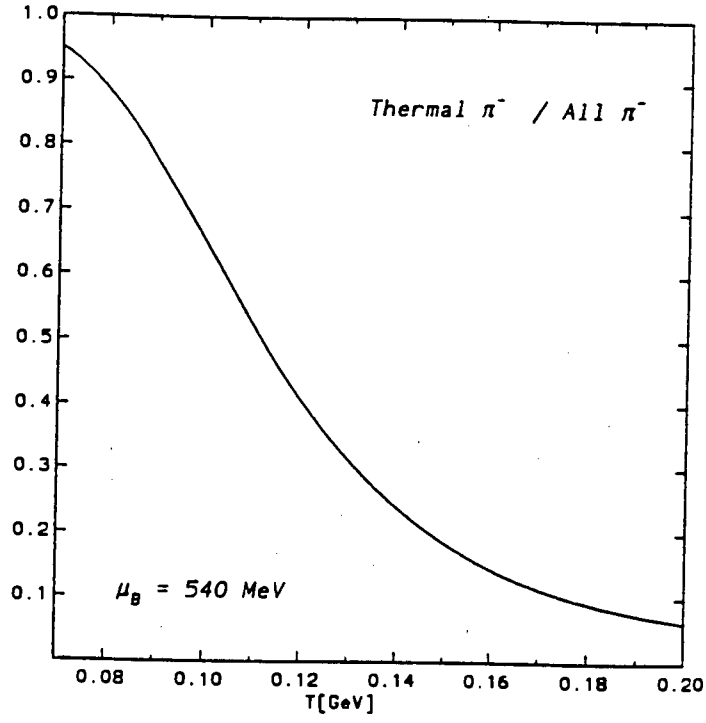

Figure 2.2: Total pions and thermal pions: Ratio of total to thermal π^-'s as a function of temperature T, calculated using the Decay Table listed in App. L. The baryon chemical potential (μ_B) is kept fixed at 540 MeV, a typical value found using the Hadron Gas model in $Si - Au$ collisions at the AGS.

p_T. However there are other explanations put forward for the low p_T anomaly namely: finite volume effects, lack of chemical equilibrium in the pions necessitating the introduction of a pion chemical potential μ_π [17].

2.4 Rapidity Spectra.

Beginning from

$$E\frac{d^3n}{d^3p} = \frac{g\lambda}{(2\pi)^3}\, m_T \cosh(y - y_{FB})\, e^{\frac{-m_T}{T}} \cosh(y - y_{FB}) \tag{2.13}$$

Integrating eq.(2.13) by parts over m_T, and using $y' = y - y_{FB}$ we find

$$\frac{dn}{dy} = \frac{g\lambda}{(2\pi)^3}\, m^2 T e^{\frac{-m}{T}} \cosh y' \left(1 + 2\left(\frac{T}{m\cosh y'}\right) + 2\left(\frac{T}{m\cosh y'}\right)^2\right) \tag{2.14}$$

The behaviour of the above equation for $m \geq T$ is

$$\frac{dn}{dy} \sim e^{\frac{-m}{2T}}\,(y - y_{FB})^2 \tag{2.15}$$

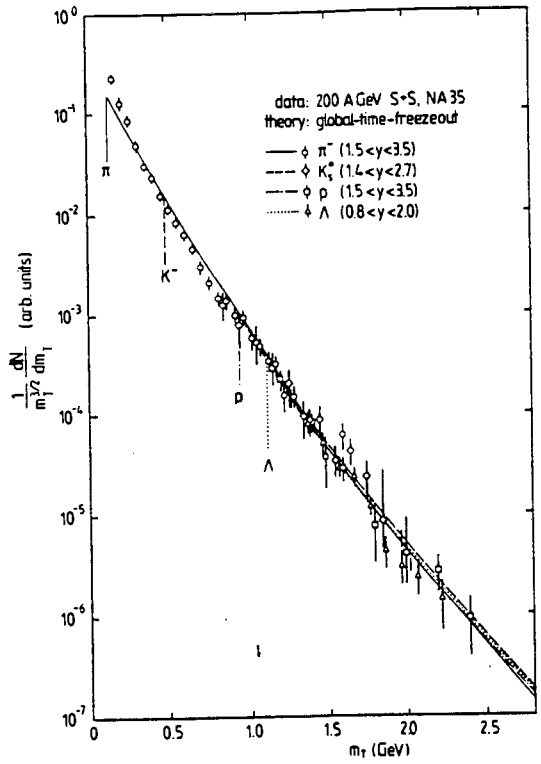

Figure 2.3: Indication of transverse flow? Concave transverse mass spectra: Transverse mass spectra for pions, kaons, protons and Λ's from central 200 A GeV $S+S$ collisions. After arbitrary normalisation all slopes agree, with the spectra falling on a universal theoretical curve for an expanding thermalised fireball [18].

The rapidity distribution of a stationary thermal fireball looks like a Gaussian centred at y_{FB}, with width

$$\Gamma_{fwhm} = \sqrt{8ln2\frac{T}{m}} \cong 2.35\sqrt{\frac{T}{m}} \tag{2.16}$$

So the rapidity spectrum has a mass-dependent width and decreases for heavier particles like $1/\sqrt{m}$. For massless particles we have $dn/dy \sim 1/(\cosh^2 y')$, roughly a Gaussian with width $\Gamma_{fwhm} \simeq 1.76$. Looking at the deviation from this limit for small (m/T)

$$\frac{dn}{dy} = \frac{g\lambda}{(2\pi)^2} T^3 \left(\frac{2}{\cosh^2 y'} + O\left(\frac{m^3}{T^3}\right)\right) \tag{2.17}$$

Here again we see that the influence of T on dn/dy is very small. When comparing the data gathered thus far from heavy ion collisions, there is not the same success as the m_T spectra. Equation (2.16) implies a narrowing in the width of the rapidity distribution for heavier particles emitted isotropically in a stationary fireball. Unfortunately, the data tells a much different story, with all the particles exhibiting rapidity distributions far wider than described in equation (2.16), indicating that the momentum distribution of the measured particles is not isotropic, but that the particles carry a memory of the momenta of the colliding nuclei. A first attempt to reproduce the measured broad rapidity distributions is to include non-thermal resonance decay particles, but it meets with little success [17]. The

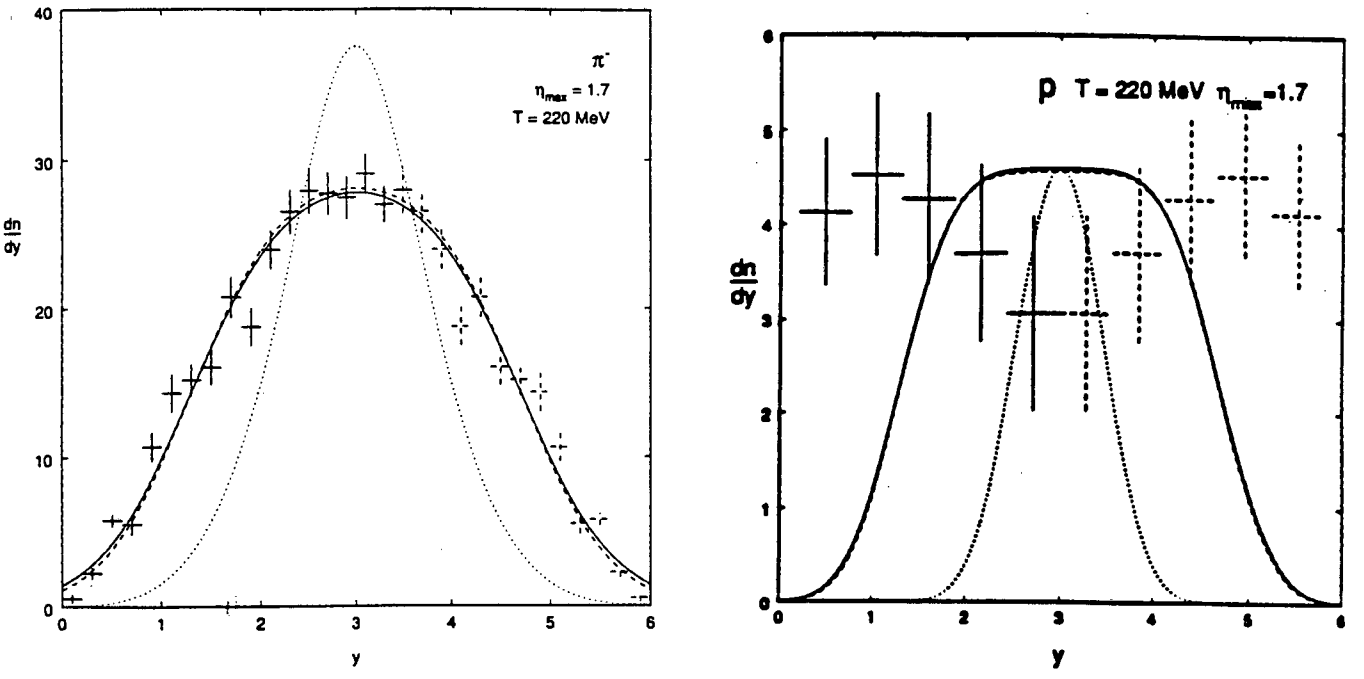

Figure 2.4: Rapidity spectra: Dotted line: Thermal π^- (left) and proton (right) rapidity spectra from a stationary fireball. Solid line: Rapidity spectra for a longitudinally expanding source. (The effect of resonances is marginal: Dashed line (absolute normalisation always adjusted for a best fit). Note 'nuclear transparency' illustrated in the proton rapidity spectrum [17].

proton rapidity spectrum is particularly alarming, showing that the protons still carry a large fraction of their collision energy, a curious phenomenon labelled 'nuclear transparency'. Similarly, all the other hadronic species have rapidity spectra that are wider than the stationary thermal fireball predicts. Thus a purely thermal picture cannot explain the rapidity spectra.

2.5 Spectra from flowing sources.

The confirmation of chemical equilibrium among emitted hadrons at freeze-out is not connected to any specific expansion pattern. In particular it does not imply isotropic emission from a single stationary fireball. Starting from a uniform medium, hydrodynamic flow preserves chemical equilibration. However, for anisotropic boundary conditions it leads to anisotropic momentum distributions (distorting chemical equilibration spectral shapes). Hence the momentum spectra of thermally emitted hadrons, and the source radii obtained from hadron-hadron interferometry are needed to determine the nature of the expansion. There is therefore ambiguity in the meaning of 'temperature' when collective flow is present. The inverse slope values obtained in the $dn_i/(m_T^{\frac{3}{2}}\, dm_T)$ vs m_T plots have assumed that there is no flow in the transverse direction; the motion is purely thermal when viewed from the

centre of mass inertial frame. Should there be flow in the transverse direction, the thermal spectral shapes will be maintained, although the inverse slope ('apparent' temperature) will be increased, depending on the mass of the particle. Absence of transverse flow is recognizable by the slopes of particles of widely differing mass being the same, as shown in the previous treatment of a stationary fireball without any collective flow. Now we allow flow in the transverse direction, and investigate its effect on the momentum distribution and subsequently 'temperature' of the hadrons. See Appendix F for a treatment of uniform transverse flow.

We end up with an interesting result

$$\lim_{(m_T/T)\to\infty} \frac{dn_i}{dm_T} \propto m_T^{\frac{3}{2}} e^{\left(\frac{-m_T}{T}\sqrt{\frac{1-v_T}{1+v_T}}\right)} \tag{2.18}$$

Comparing eq.(2.18) with eq.(2.12) we can recover an 'apparent' temperature, T_{app} for transverse flow where

$$T_{\text{app}} = T\sqrt{\frac{1+v_T}{1-v_T}} \tag{2.19}$$

This basic treatment of transverse flow relates the 'apparent' temperature to a constant transverse expansion velocity. According to equation (2.19), transverse expansion always *increases* the 'temperature' (decreases the slope), and hence is termed a 'blueshift' factor to the actual temperature. Since in general, the transverse velocity is not a constant, but has a transverse radial profile, spectra with different 'blueshift' factors are superimposed in the total spectrum. At large m_T the 'blueshift' factor corresponding to the largest expansion velocity across the freeze-out surface dominates, and thus dictates the asymptotic fall-off of the m_T spectrum. In the intermediate m_T region the superposition of spectra with different 'blueshift' factors leads to a clearly visible concave curvature of the m_T spectra (see Fig.(2.3)). This feature is interpreted as a characteristic consequence of collective transverse flow. So transverse flow increases the 'apparent' temperature. Intuitively this seems correct, as m_T will gain from the radial boost, with the more massive particles and resonances showing the largest increase in m_T. Therefore transverse flow is often used as a model to recover the intrinsic temperature when the slopes of particles of differing mass differ systematically.

2.6 Longitudinal flow.

We look to longitudinal flow to explain the width of the rapidity plots. Invoking the boost-invariant Bjorken longitudinal expansion model [7], with some modifications, we try to explain the longitudinal momentum distributions. The Bjorken model describes the

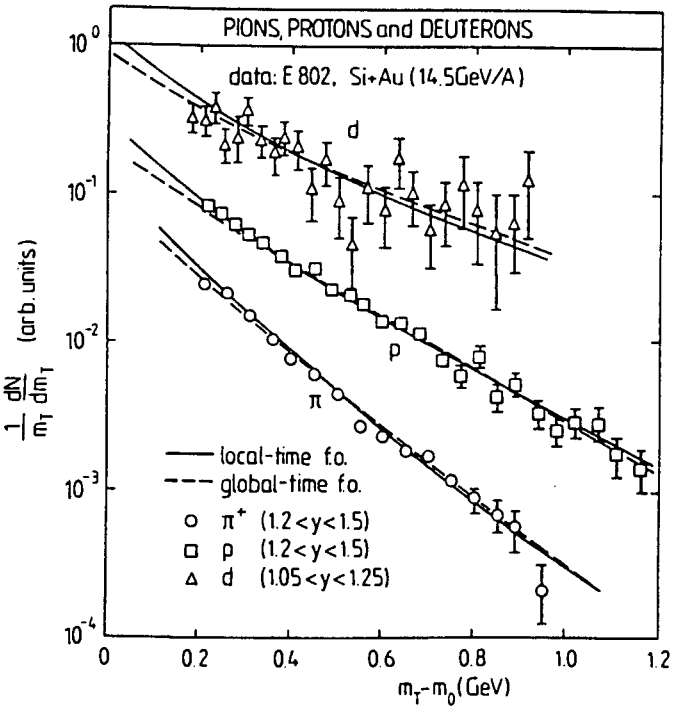

Figure 2.5: Increase in 'apparent' temperature: Flattening of slopes at high m_T. Comparison of the theoretical spectra with E802 $Si - Au$ data [19].

collision of two highly Lorentz-contracted incident nuclei, viewed as approaching 'pancakes', followed by receding 'pancakes' carrying the baryon number, whilst a central region of zero net baryon number exists between the two 'pancakes'. The model can explain anisotropy at the level of particle production, after expansion leads to boost-invariant longitudinal flow of matter with locally thermalised distributions. However, the model is formulated for asymptotically high energies, where the rapidty distribution shows a central plateau at midrapidity [20]. At the current energies, we find half the total rapidity gap is wolfed up by the target and projectile fragmentation regions, leaving the pion distribution more like a Gaussian than a central plateau shape. The boost-invariant scenario is modified [21] to account for the limited available beam energy by restricting the rapidity η to the interval (η_{min}, η_{max}). the rapidity distribution is then the integral over the uniformly distributed thermal sources

$$\frac{dn}{dy} = \int_{\eta_{min}}^{\eta_{max}} d\eta \frac{dn_{th}}{dy}(y-\eta) \tag{2.20}$$

where

$$\frac{dn_{th}}{dy} = \frac{g\lambda}{(2\pi)^3} m^2 T e^{\frac{-m}{T}} \cosh y' \left(1 + 2\left(\frac{T}{m\cosh y'}\right) + 2\left(\frac{T}{m\cosh y'}\right)^2\right) \tag{2.21}$$

The transverse mass spectrum is not affected by this operation, a further illustration of of the usefulness of the variables y and m_T. The shape of the transverse mass spectrum is

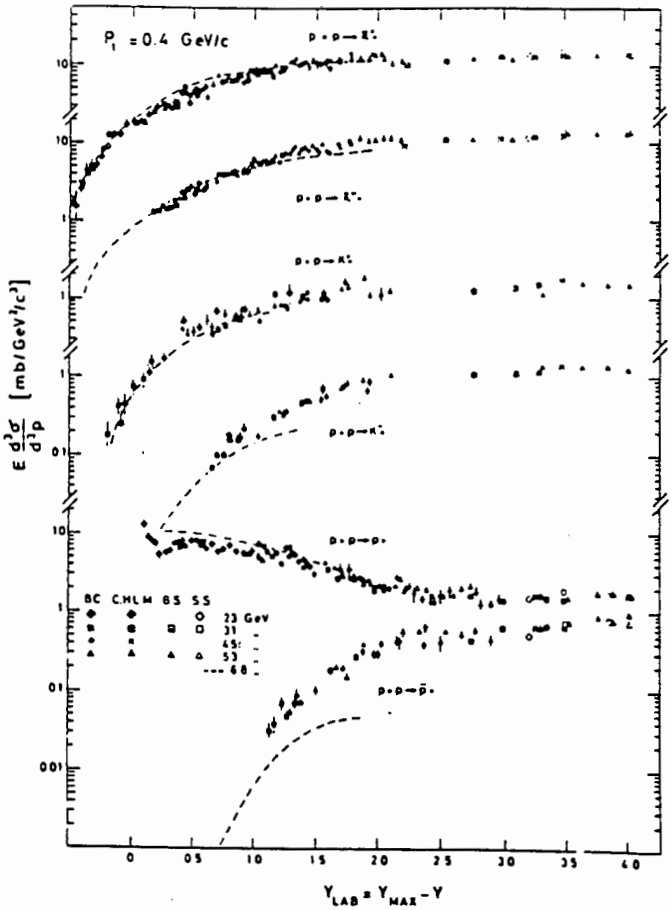

Figure 2.6: Central plateau in rapidity spectra: ISR data showing the plateau in the central region of rapidity and the particle yields [20].

primarily dictated by the temperature T and the transverse flow rapidity y_T. The longitudinal flow velocity y_L determines the rapidity spectrum which, in turn, shows very little sensitivity to T and practically none to transverse flow. Fits are done to the measured rapidity spectra using $\eta_{max} = -\eta_{min}$ as the single free parameter (the fits are not sensitive to temperature T). There is mild success. The measured proton rapidity spectrum shows the 'nuclear transparency'. Because there is no clearcut region between the central and fragmentation regions in the experimental y spectrum, we would expect the model to fall short. The produced strange particles' rapidity spectra are better reproduced, although the Λ's exhibit some similarity to the protons. The produced strange particles are good indicators of collective flow, not being particles of the original nuclei and thus uncontaminated by a cold spectator component (unlike the protons). Furthermore, their larger mass accentuates their flow component against the thermal background. Also, a best fit of the hadronic rapidity spectra can be done for each particle species, by adjusting η_{max} for each species. The results agree very well with the analysis above, and highlight the protons' memory of the colliding nuclei.

One can conclude that the rapidity distributions are quite reasonably described in terms of a sizeable collective longitudinal flow at freeze-out. Why then should there not be some transverse flow?

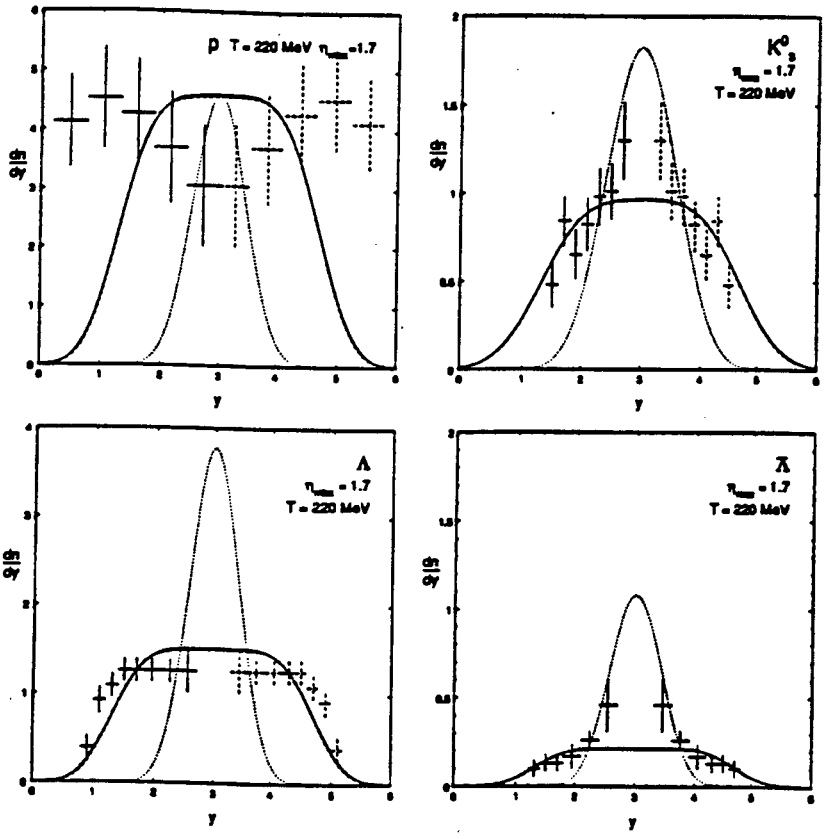

Figure 2.7: Rapidity interval cutoff: Attempt to reconcile the Hadron Gas model with the measured rapidity spectra. All solid lines are rapidity spectra allowing longitudinal flow and using $\eta_{max} = 1.7$ (see text) [17].

2.7 Conclusion.

The extension of the stationary thermal model by including resonance decays and a longitudinal flow component, and a tentative inclusion of transverse flow, has provided a phenomenological description of almost all spectra, and the remaining exceptions highlight the limitations of the model. However, this seemingly complete picture of the dynamics of the hadronic matter has some serious intrinsic theoretical problems:

1) At $T \sim 200$ MeV, the mean free path of pions in hadronic matter is much less than 1 fm (estimated from the thermal distributions and averaged cross-sections of pions with nucleons and with each other [22]. However, the size and the lifetime of the reaction region is several fm, as can be guessed from the radius of the projectile (S, Si etc). The length of the collision zone will be even larger because of the time dilation factors of the relativistic longitudinal expansion stretch the system quite long already during the formation time $\tau_f \simeq 1$ fm/c. Consequently, the pions cannot leave the interaction zone at $T \sim 200$ MeV without further collisions. The reaction region cannot decouple thermally and should, by continuing expansion force the pions to cool down further.

2) The longitudinal expansion of the boost-invariant scenario corresponds to a solution of

the hydrodynamical equations in (1+1) dimensions. i.e.

$$u_\mu(\tau, y) = (u_0(\tau, y), 0, 0, u_z(\tau, y)) \tag{2.22}$$

presumably the one-dimensional expansion dominates initially because of the initial conditions (boost in one dimension only). But it is inconsistent to assume that a thermalised system expands collectively in a longitudinal direction without generating transverse flow from the high pressures in the hydrodynamic system. Maintaining azimuthal symmetry would require (2+1) dimensions. Transverse expansion will also increase the cooling rate.
3) Transverse velocities of 0.3 - 0.6c (moderate when compared with the longitudinal expansion with a $\beta_L = \tanh \eta_{max} \geq 0.9$c) could change the transverse mass spectra considerably, by enhancing the particle yields at high m_T, similarly depressing the yields at low m_T. Since the entire stationary spectra would be boosted, the effect would be smaller in the lighter particles, but very noticeable in the heavier ones.

2.8 A last word on transverse flow and the thermal model.

Until very recently, the evidence for transverse flow was regarded as purely circumstantial [23]. However, there is some support for the evidence of transverse flow effects, obtained in an analysis of azimuthal distributions of transverse energy [24] in semi-central $Au - Au$ collisions at AGS energies. This will have to be looked at very closely. An agreed transverse flow signal has not yet emerged from the data gained from nuclear collisions. From phenomenology alone there is no need for an additional transverse flow effect, since all the data have already been described reasonably well. Currently we thus will not be able to prove the existence of transverse flow from the data alone. Only an indirect proof based on the phenomenological analysis together with hydrodynamical calculations with a consistent theoretical treatment of the freeze-out processes, can be given.
However, in the near future larger collision systems are expected, which will lead to an increase in collective effects, perhaps testifying to transverse degrees of freedom other than purely thermal ones.
As a final note on the subject of transverse flow in the Hadron Gas model it has been shown that the ratios of particle densities are independent of the transverse flow [25]. An outline of this proof is given in Appendix K.

Chapter 3

Application of the Hadron Gas model to $Si - Au$ data

3.1 Introduction.

As mentioned in Chapter 2, unambiguous tests for thermalisation exist so far only for the final hadronic stage of the products of nuclear collisions. To conclude that strongly interacting matter can be produced by nuclear collisions we must show that the most abundantly observed hadrons produced by these collisions were emitted from a thermal source [26, 27]. The experimental study of thermalisation is therefore of fundamental importance. We seek to examine the experimental data, within the Hadron Gas formalism, for evidence of thermalisation, the signatures of which have been reviewed in the previous chapter.
In the fullest compliance to the thermal composition laws, we would see 'chemical equilibrium' (abundances of different hadron species at freeze-out is specified by the freeze-out parameters T and μ_B). It has been noted that hadrons of a given species could be in local *thermal* equilibrium even though *chemical* equilibrium between the different species is not attained [28]. A recent comprehensive analysis of BNL-AGS data from $Si-Au$ collisions [29, 30] provides first evidence that the most abundantly observed hadrons were indeed emitted from a thermal source. If supported by further results from $Au-Au$ collisions at the AGS and at higher energies from the CERN-SPS, this conclusion would be the decisive step in showing that strongly interacting *matter* can be produced by nuclear collisions. In view of the importance of such a result, we find it useful to analyse the present AGS data independently in a self-contained hadrosynthesis approach. Our analysis will be based solely on particle ratios, *without* any source volume or flow features, and it will take into account the initial state isospin asymmetry [53].

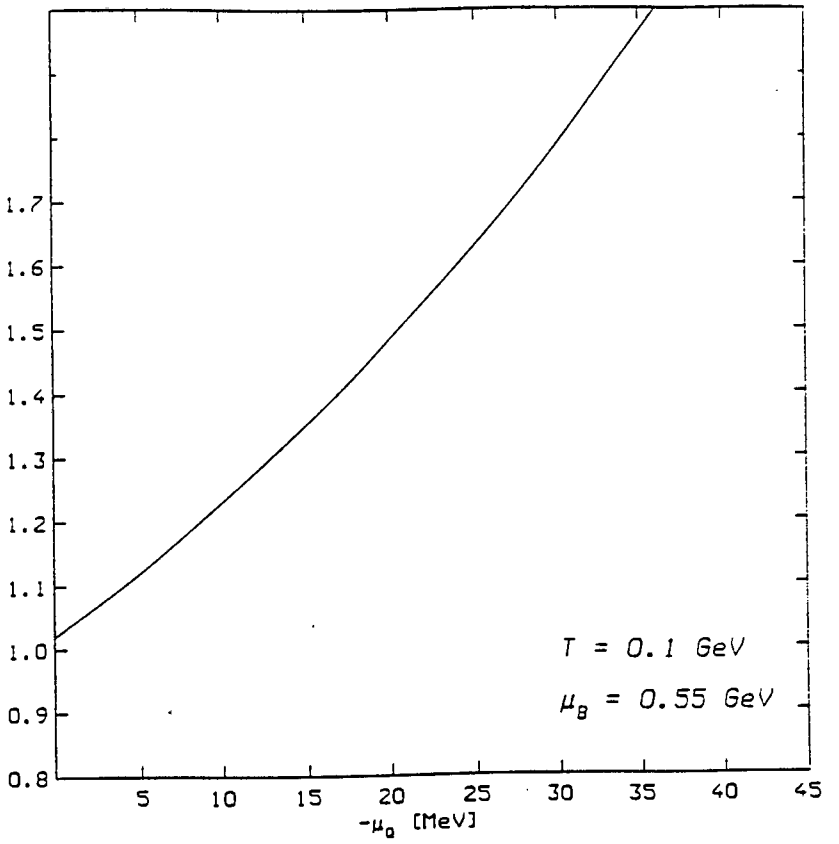

Figure 3.1: The π^-/π^+ ratio of an ideal gas of hadrons and hadronic resonances at freeze-out as a function of charge chemical potential μ_Q at fixed freeze-out parameters $T^F = 100$ MeV, $\mu_B^F = 550$ MeV.

3.2 Overall Charge Conservation.

If the initial state contains more neutrons than protons, as in the Si–Au case, it is necessary to introduce a further chemical potential μ_Q.

An excess of neutrons in the initial state translates, at the quark level, into an excess of d quarks, manifesting in e.g. a π^-/π^+ ratio different from unity. (The π^-, a $\overline{u}d$ quark combination, profits from the greater density of d quarks). For isotopic symmetric nuclear matter, $(Q/B = 0.5)$ one finds that $\mu_Q = 0$. In this regard see Appendix G. This zero value of μ_Q is the reason why it has previously attracted so little attention. As we move to $Au - Au$ and $Pb - Pb$ collisions there is greater isospin asymmetry, so best we incorporate a charge chemical potential to ensure overall charge conservation.

The analysis presented below takes such deviations from an isospin-symmetric initial state fully into account. Since the neutron/proton and the π^-/π^+ ratios deviate from one by about ten to twenty percent, the results from this analysis will generally differ from the isospin-symmetric case by this order of magnitude. Estimates of the effects of a charge chemical potential have been presented previously [31, 32], but no quantitative treatment of experimental data has taken place.

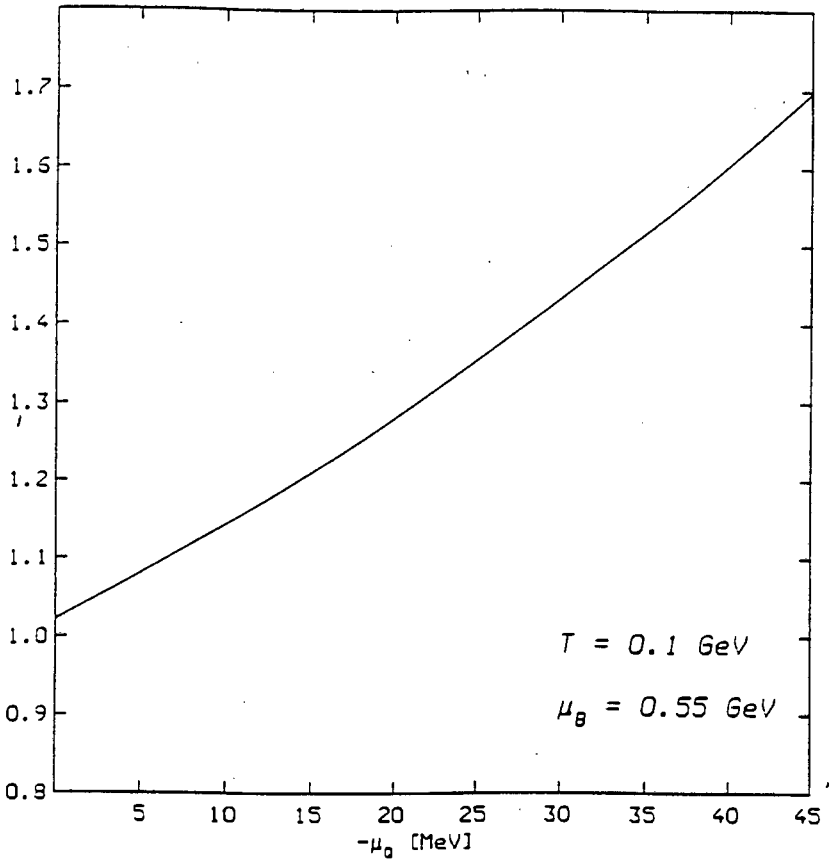

Figure 3.2: The neutron/proton ratio of an ideal gas of hadrons and hadronic resonances at freeze-out as a function of charge chemical potential μ_Q at fixed freeze-out parameters $T^F = 100$ MeV, $\mu_B^F = 550$ MeV.

3.3 Hadronic Ratios.

The measured hadron production ratios listed in Table (3.1) form the basis of our analysis. If the hadrons are emitted from a source in full chemical equilibrium, each measured ratio determines a range of $T - \mu_B$ values with which it is compatible. This range can be calculated on the basis of an ideal gas of all observed hadrons and hadronic resonances, requiring overall charge and strangeness conservation and taking into account resonance decays [26]. Let me outline the method. If at freeze-out we have an ideal gas of hadrons and hadronic resonances, then the system is described by the partition function

$$\ln Z(T, \mu_B, \mu_S, \mu_Q) = \sum_i \lambda_B^{B_i} \lambda_S^{S_i} \lambda_Q^{Q_i} W_i \tag{3.1}$$

As outlined in Chapter 2, W_i is the phase space factor for hadrons of species i (mesons, baryons and their antiparticles), with S_i, B_i and Q_i denoting the strangeness, baryon number and charge of the hadron in question. The difference between quantum and Boltzmann statistics is negligible when the temperature of the fireball approaches 100 MeV, a value our freeze-out temperatures exceed. The phase space factors, using Boltzmann statistics, are given by

$$W_i = \frac{g_i m_i^2 VT}{2\pi^2} K_2\left(\frac{m_i}{T}\right) \tag{3.2}$$

with g_i denoting the spin degeneracy, m_i the mass of hadron species i; V is the volume of the system. We include in the sums in eq.(3.1) all hadrons listed in the latest Particle Data Compilation [34], excluding charm and bottom resonances; decays are taken into account with their experimental branching ratios, with an educated guess being made whenever the information on decays is not complete. The resulting table contains 479 entries and is listed in Appendix L. The partition function (3.1) then determines all thermal properties of the system in terms of the four parameters T, μ_B, μ_S and μ_Q. The chemical potential for the strangeness, μ_S, can be fixed by requiring the overall strangeness of the system to vanish. Similarly, the chemical potential for the charge, μ_Q, is fixed by requiring the charge/baryon ratio of the final state to be equal to that of the initial state. If there is a one-stage freeze-out of all thermal hadrons, then all production ratios (π/p, K/π, $K/\bar{K}$, ρ/π, ϕ/π, $Y/p, ...$) are given in terms of the two remaining parameters T, and μ_B. For example, we can use the measured π^+/p and K^+/π^+ ratios to fix the values of T and μ_B; all other ratios are then predicted, if the different particle species are indeed present according to their equilibrium weights.

To fix the overall charge/baryon ratio, we thus have to estimate the number of interacting protons and neutrons in the initial state. For a central A–B collision ($A \ll B$), the number $N_{\rm part}$ of participant nucleons is the sum of the nucleons in A and those in a tube of radius R_A through nucleus B,

$$N_{\rm part} \simeq [A + (\pi R_A^2) n_0 2R_B] \simeq [A + 1.5A^{2/3}B^{1/3}] \tag{3.3}$$

See Appendix H for a derivation of the above equation. Here $n_0 = 0.17$ fm^{-3} is standard nuclear density; $R_A = 1.12A^{1/3}$, and similarly for B. For $Si-Au$ collisions, we thus obtain $N_{\rm part} \simeq 108$. With $Z/A = 0.5$ for Si and $Z/A = 0.4$ for Au, this is made up of $N_p \simeq 46$ protons and $N_n \simeq 62$ neutrons. We thus have to fix the overall charge/baryon of the final state at 46/108 by suitably adjusting the charge potential μ_Q at the temperature T and baryochemical potential μ_B obtained from particle ratios. As noted, the strangeness potential μ_S is fixed to give the final state a vanishing overall strangeness.

3.4 Results.

We begin with the most abundantly observed hadron species, p, $\pi^\pm$, $K^\pm$ and Λ, since these are most likely to be thermalised. What we denote by Λ will always include the Σ^0, since the two are experimentally not separable. From the production rates of these six hadron species, we get five independent ratios. As seen in Fig.(3.3), four of these in fact cross in a common region in the plane of temperature and baryochemical potential, so that pions,

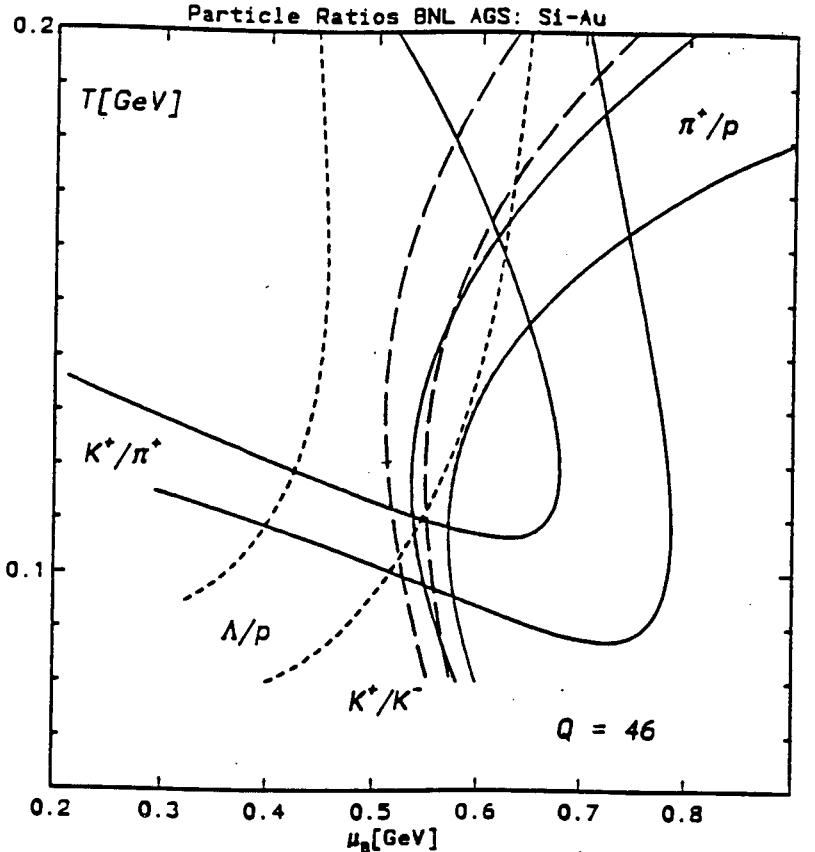

Figure 3.3: The $T - \mu_B$ regions determined by the indicated particle ratios (including experimental errors). The charge is kept fixed at 46, corresponding to 46 participant protons and 62 participant neutrons.

nucleons, kaons, antikaons and lambdas are observed according to their thermal weights. Fig.(3.4) is a magnification of Fig.(3.3) highlighting the common region. The freeze-out parameters thus obtained are

$$T_F = 110 \pm 5 \text{ MeV} \qquad \mu_B^F = 540 \pm 20 \text{ MeV} \tag{3.4}$$

The fifth ratio, which can be taken either as the K^-/π^- or the π^-/π^+ ratio, is also in agreement with the above values. In Fig.(3.5) we show that when charge conservation is not enforced (i.e. the isospin-symmetric case, with $\mu_Q = 0$), there is never a consistency between the π^+/p and K^+/K^- experimental ratios. The additional constraint of charge conservation, normalized by the initial state participating nucleons, provides an overlap region for these experimental ratios, allowing a consistent set of thermodynamic parameters to be determined. Our model gives a freeze-out radius of $R^F \sim 7.5$ fm, and at this scale for R^F we have checked that the finite volume corrections [35] discussed in [29] do not modify our results, by recalculating Fig.(3.3) and noting no modification to the coordinates where the ratios overlap. See Appendix I. The corresponding baryon density is $n_B = 0.057 \pm 0.025$ fm^{-3} and hence about 1/3 standard nuclear density, indicating considerable expansion before freeze-out.

A full discussion of the results, and comparison with the literature on the $Si - Au$ collisions follows in the next chapter. Below follows an explanation of the tables produced, with a

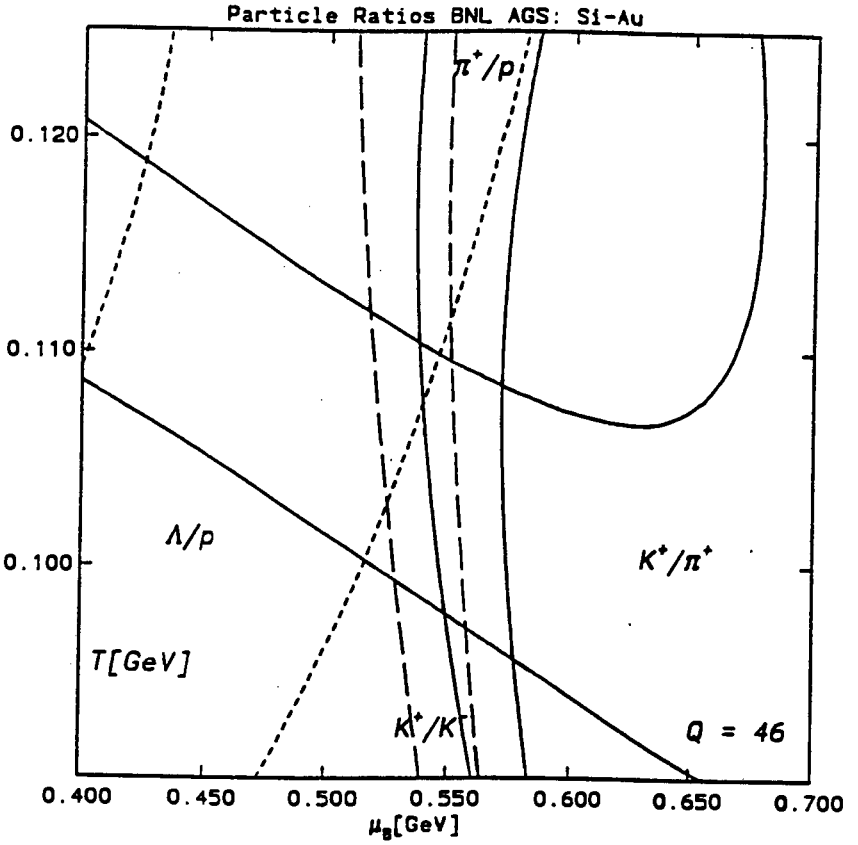

Figure 3.4: Magnification of the $T - \mu_B$ regions determined by the indicated particle ratios (including experimental errors). The charge chemical potential in the overlapping region is -8 MeV.

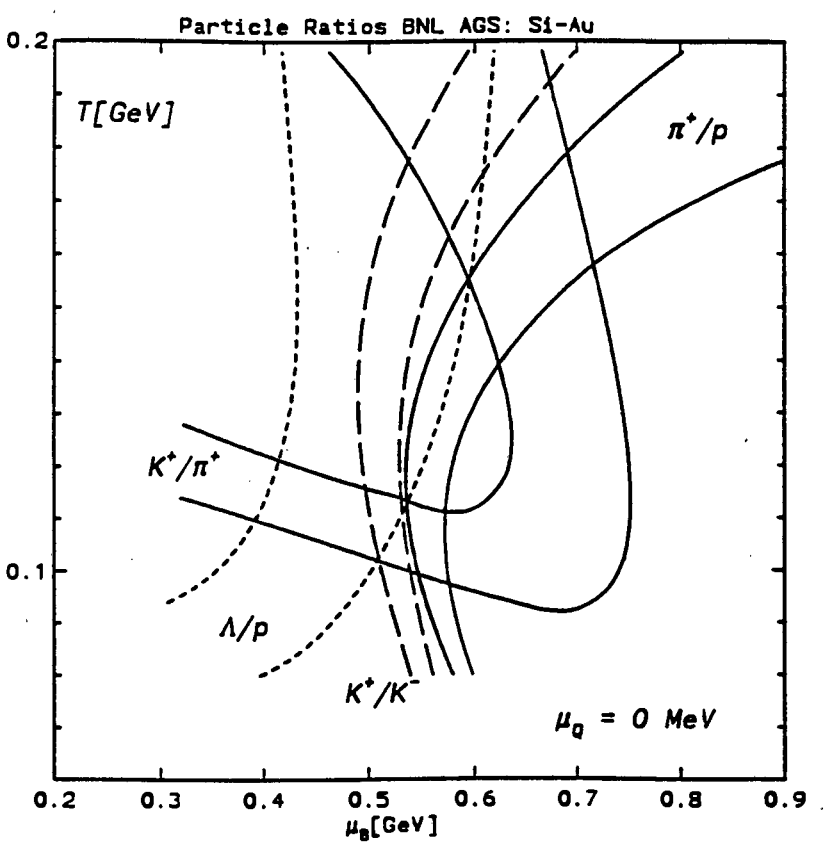

Figure 3.5: The $T - \mu_B$ regions determined by the indicated particle ratios (including experimental errors). The charge chemical potential is taken to be zero, thus neglecting the isospin asymmetry of the initial state.

brief comment on the results that the tables display.

In Table (3.1), we list all thermal ratios as determined by these values, together with the measured ratios. It is evident that the emission rates of nucleons, pions, kaons, antikaons and hyperons are correctly described by thermal composition.

Given the initial state baryon number of 108, we can extract from the ratios of Table (3.1) the thermal abundances of the different species; they are listed in Table (3.2). Also shown there are the experimental abundances, obtained in the same way from the experimental ratios.

Next we turn to less copiously produced hadron species. In Table (3.1), we also list their measured ratios together with the corresponding predictions from thermal emission at the freeze-out parameters (3.4). We see that the value for ϕ production [36] agrees well 0.1 ϕ's per event. Multiply strange baryons (Ξ) are experimentally more abundant than thermally predicted. A definite disagreement with the thermal predictions is found for antibaryons ($\bar{p}$ and $\bar{\Lambda}$): these are produced much more copiously than their thermal predictions.

From Fig.(3.3) another region of overlapping ratios is of interest. All the ratios, excepting the K^+/K^- ratio which is out by a further standard deviation, overlap at

$$T_F = 160 \pm 5 \text{ MeV} \qquad \mu_B^F = 620 \pm 20 \text{ MeV} \tag{3.5}$$

Performing the same analysis as outlined above, but using freeze-out parameters (3.5) results in Tables (3.3) and (3.4). At a quick glance freeze-out parameters (3.5) fare better than those in (3.4) in reproducing the rarer strange and antibaryon particle numbers. However, freeze-out parameters (3.5) yield a freeze-out baryon density of $n_B = 0.33 \pm 0.15$ fm^{-3}, hence about *twice* standard nuclear density of 0.17 fm^{-3}. This seems unphysical, and exposes our model of neglecting to ensure that a limiting 'excluded' volume is reached in the limit of very high baryon density (see Appendix J). For a system of colliding nuclei to freeze-out (i.e. cease to interact strongly) when the hadrons are closer to one another than in normal nuclear matter is unlikely.

Table 3.1: Ratios of Hadron Species in Si-Au Collisions at the AGS (Thermal parameters: $T = 110 \pm 5$ MeV, $\mu_B = 540 \pm 20$ MeV).

Particle Ratio	Experimental Ratio	Thermal Ratio
π^+/p	0.80 ± 0.08	0.87 ± 0.15
K^+/π^+	0.19 ± 0.02	0.21 ± 0.02
K^+/K^-	4.40 ± 0.40	4.51 ± 0.62
Λ/p	0.20 ± 0.04	0.16 ± 0.02
K^-/π^-	$0.035 \pm .005$	0.038 ± 0.006
Ξ^-/Λ	$(1.2 \pm 0.2) \times 10^{-1}$	$(4.9 \pm 0.5) \times 10^{-2}$
ϕ/π^+	$(4.5 \pm 1.2) \times 10^{-3}$	$(4.6 \pm 1.3) \times 10^{-3}$
$\bar{p}/p$	$(4.5 \pm 0.4) \times 10^{-4}$	$(7.2 \pm 6.3) \times 10^{-5}$
$\bar{\Lambda}/\Lambda$	$(2.0 \pm 0.8) \times 10^{-3}$	$(3.4 \pm 3.0) \times 10^{-4}$

Table 3.2: Abundances of Hadron Species in Si-Au Collisions at the AGS (Thermal parameters: $T = 110 \pm 5$ MeV, $\mu_B = 540 \pm 20$ MeV).

Particle Species	Experimental Numbers	Thermal Numbers
nucleons	94	94
pions	120	133
kaons	14	17
hyperons	14	12
antikaons	3	4
Ξ's	2	1
ϕ's	2×10^{-1}	2×10^{-1}
antinucleons	4×10^{-2}	6×10^{-3}
antihyperons	3×10^{-2}	4×10^{-3}

Table 3.3: Ratios of Hadron Species in Si-Au Collisions at the AGS (Thermal parameters: $T = 160 \pm 5$ MeV, $\mu_B = 620 \pm 20$ MeV).

Particle Ratio	Experimental Ratio	Thermal Ratio
π^+/p	0.80 ± 0.08	0.86 ± 0.07
K^+/π^+	0.19 ± 0.02	0.21 ± 0.01
K^+/K^-	4.40 ± 0.40	5.10 ± 0.57
Λ/p	0.20 ± 0.04	0.16 ± 0.01
K^-/π^-	$0.035 \pm .005$	0.036 ± 0.004
Ξ^-/Λ	$(1.2 \pm 0.2) \times 10^{-1}$	$(4.7 \pm 0.3) \times 10^{-2}$
ϕ/π^+	$(4.5 \pm 1.2) \times 10^{-3}$	$(9.1 \pm 1.0) \times 10^{-3}$
$\bar{p}/p$	$(4.5 \pm 0.4) \times 10^{-4}$	$(7.0 \pm 4.1) \times 10^{-4}$
$\bar{\Lambda}/\Lambda$	$(2.0 \pm 0.8) \times 10^{-3}$	$(6.7 \pm 2.9) \times 10^{-3}$

Table 3.4: Abundances of Hadron Species in Si-Au Collisions at the AGS (Thermal parameters: $T = 160 \pm 5$ MeV, $\mu_B = 620 \pm 20$ MeV).

Particle Species	Experimental Numbers	Thermal Numbers
nucleons	94	95
pions	120	125
kaons	14	16
hyperons	14	11
antikaons	3	3
Ξ's	2	1
ϕ's	2×10^{-1}	3×10^{-1}
antinucleons	4×10^{-2}	6×10^{-2}
antihyperons	3×10^{-2}	7×10^{-2}

Chapter 4

Review of Si-Au thermal model literature

4.1 Thermalisation.

Thermalisation in the AGS energy range can lead to an increase, or to a *decrease* of hadron abundances relative to those measured in $p-p$ or $p-A$ interactions. Let me note three examples in some detail.

1) A well documented case is shown in Fig.(4.1): the K^+/π^+ ratio [37]. It grows from a $p-p$ value near 0.05 to a four times larger thermal value, above 0.2, in central $Si-Au$ and $Au-Au$ collisions [38, 39]). 2) Similarly, the ϕ/π^+ ratio increases by more than a factor two from its $p-p$ value to the thermal result found in $Si-Au$ data [40].

3) In contrast, the number of pions produced per participating nucleon decreases at AGS energy towards its thermal value. In Fig.(4.2), we show the $\pi/N_{\rm part}$ ratio in $p-A$ collisions at 14.6 GeV beam momentum [41]. To obtain these values, we approximate the pion multiplicity by $3\langle h_-\rangle$, where $\langle h_-\rangle$ is the average number of negative hadrons; $\pi/N_{\rm part}$ is defined as the average number of participants in a $p-A$ collision. The ratio $\pi/N_{\rm part}$ is seen to be A-independent; it remains constant at 1.5 ± 0.2 over the whole range from $p-N$ to $p-Au$. To obtain the corresponding experimental value of $\pi/N_{\rm part}$ for $Si-Au$ collisions, we multiply the measured π^+/p ratio by 3×1.14 (where the factor 1.14 accounts for the observed π^-/π^+ ratio [42]) and divide it by 2.35 in accord with 46 participating protons and 62 neutrons. We thus find a significantly lower value, 1.15 ± 0.12, which is in accord with the thermal value $133/108\simeq1.23$. This lower value is also supported by data from $Si-Al$ collisions [41]. The ratio $\pi/N_{\rm part}$ thus decreases from its $p-A$ value of about 1.5 to a somewhat lower value.

Because of enhanced annihilation chances, the ratio of antibaryon to baryon production is also expected to decrease in a dense baryonic medium. In support of this, the $\bar{p}/p$ ratio appears to decrease in going from $p-p$ to $A-B$ [43].

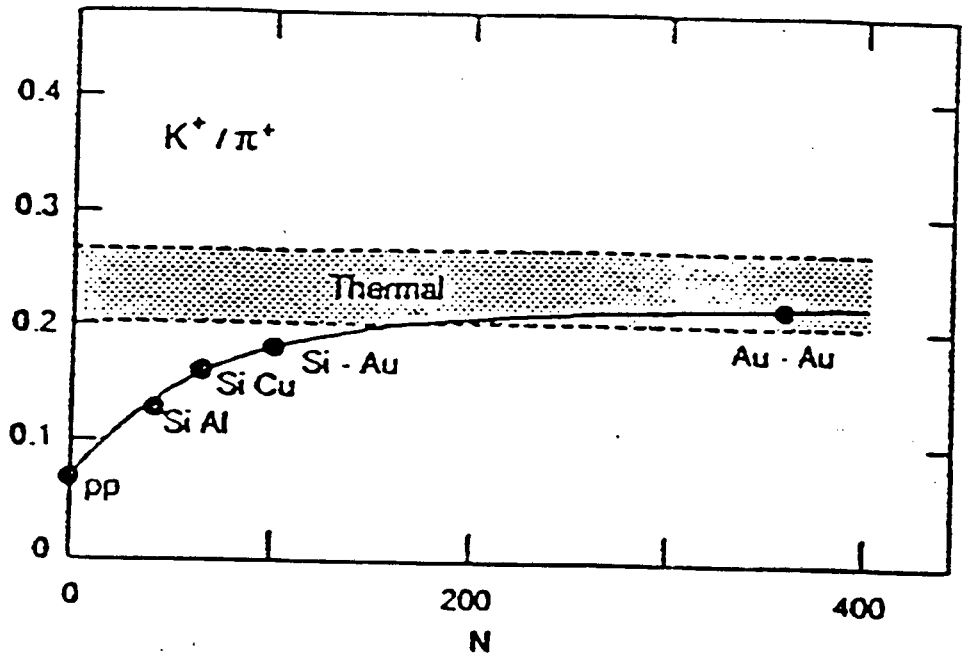

Figure 4.1: Hand drawn plot of K^+/π^+ ratios as function number of participating nucleons at AGS energies [37].

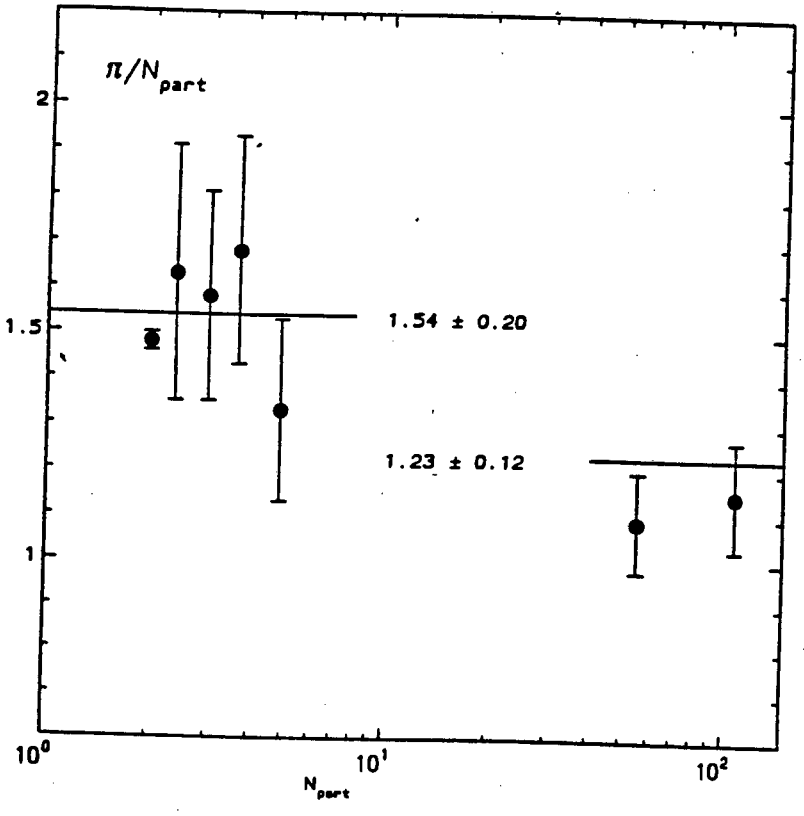

Figure 4.2: The ratio of pions to participating nucleons in $p - A$ collisions.

There is also no particular reason why all ratios should approach thermalisation by the same mechanism or at the same rate. Pion-nucleon and pion-pion interactions result in more abundant kaon production than nucleon-nucleon interactions; thus an environment with more such collisions will drive the kaon to pion ratio up. In nucleus-nucleus collisions, some of the available energy is needed to thermalise the participating nucleons and therefore is removed from meson production [44]; hence at the AGS, with very limited energy, π/N decreases to its thermal limit. As mentioned, antinucleons are more readily absorbed in nuclear matter, so that the $\bar{p}/p$ and $\bar{\Lambda}/\Lambda$ ratios in nuclear collisions are expected to be smaller than in $p-p$ interactions. And in general one would expect the approach to be slower for less copiously produced particles. The onset of thermalisation will therefore be quite specific for different species, making a final uniform thermal distribution all the more striking.

In view of the general evolution towards thermalisation, it seems misleading to single out enhanced kaon/pion or hyperon/nucleon ratios as 'strangeness enhancement'. There are fewer pions per nucleon in nucleus-nucleus collisions than in $p-p$ or $p-A$ interactions: this alone would drive the K/π ratio up, even for constant kaon production. Moreover, there are strange hadron species (e.g., antikaons) whose thermal production rate is smaller than that in hadron-hadron collisions, and there are non-strange species (e.g., Δ's) with enhanced thermal production.

We return now to the discrepancy between experimental and thermal antibaryon production. The thermal rates are determined by the dependence on the baryochemical potential μ_B: increasing μ_B at fixed temperature decreases the ratio $\bar{p}/p$ as $\lambda_B^{-2} = \exp(-2\mu_B/T)$. However, such a suppression presupposes that the antibaryons can really experience the thermal medium, and that appears not clear. The fate of antiprotons in nuclear matter has been studied in detail in low energy $p-A$ interactions [45]. Here one also expects enhanced annihilation, particularly in the production of very slow $\bar{p}$'s, which spend a long time in the medium. In contrast, one finds that over a large momentum range down to 0.5 GeV/c, the antiprotons apparently do not interact with the medium. This has been interpreted in terms of a very long formation time for baryon-antibaryon pairs in nuclear collisions, so that antiprotons emerge as well-defined particles only after leaving the nucleus [46]. It has also been considered as the effect of a specific screening of antiprotons in nuclear matter [47]. In any case, until the considerable transparency of nuclear matter for antiprotons is understood, it is not clear what role they will play in the medium produced in nucleus-nucleus collisions. It thus seems safest to exclude them from thermal considerations of AGS data, which are in the energy range studied in the mentioned $p-A$ collisions [45].

4.2 Review of $Si - Au$ Hadron Gas literature.

First of all, it must be stressed that freeze-out values

$$T_F = 110 \pm 5 \text{ MeV} \qquad \mu_B^F = 540 \pm 20 \text{ MeV}. \tag{4.1}$$

determined in [53] agree with those determined in [29]; our temperature is slightly lower [53]. Their paper [29] follows up on an earlier (1989) paper [33], which was based on the first AGS and SPS data, where the authors concluded that a high degree of thermalisation is reached, and that there is evidence for hydrodynamic expansion of the created fireball. In their very thorough 1995 paper [29] they discuss quantitatively, with the much larger set of data from $Si - Au$ collisions, the validity of the thermodynamic approach in interpreting the data. Using basically the same formalism as [48, 26], but this time armed with a fuller set of data, the quantitative predictions of a self-consistent thermodynamic and hydrodynamic approach are explored within a fireball scenario [31, 51]. However, the setting of the parameters of the Hadron Gas model differs from our overlapping ratios technique.
Unlike [49], chemical equilibrium is used throughout combined with strangeness conservation. No effort is made to conserve the overall charge of the fireball. Similarly using a grand canonical ensemble of non-interacting fermions and bosons in equilibrium at freeze-out, but, arguing that the system is of finite size, their grand canonical equation is multiplied by a correction factor [35] which is evaluated for a spherical volume with radius R (see Appendix I). For the freeze-out values listed in equation (4.1) above, this correction factor is essentially negligible [53]. Also, an excluded volume correction is applied [31] , with the baryonic and mesonic radii fixed at 0.8 and 0.6 fm respectively (see Appendix J).
Arguing that the relevant temperature range of 100 - 150 MeV sets a scale for the mass range of particles to be considered, they include strange and non-strange mesons up to 1.5 GeV, and baryons up to 2 GeV. In our work we included all meson (excluding charm) and baryon decays in the Particle Data Compilation [34], and then explored the effects of a cut-off mass on the ratios of particles. The K^+/π^+ was the most sensitive to cut-off mass of the four ratios we used to fix the freeze-out parameters. For the temperatures within the 100 - 150 MeV range, it appears from our plot shown in Fig.(4.3) that the cut-off masses used in [29] are very reasonable for the energies at the AGS.
The fixing of the model parameters differs greatly to our overlapping particle ratios technique [53]. In [29], the temperature range for freeze-out was fixed by a study of Δ production. However, the determination of the Δ yield is quite delicate, based on pion transverse momentum distributions at small p_T and/or reconstruction over a partially known background [50]. To avoid the uncertainties this leads to, we use the directly measured hadron ratios. For the freeze-out parameters (4.1), we get an overall thermal ratio $\Delta/N = 0.25 \pm 0.02$.

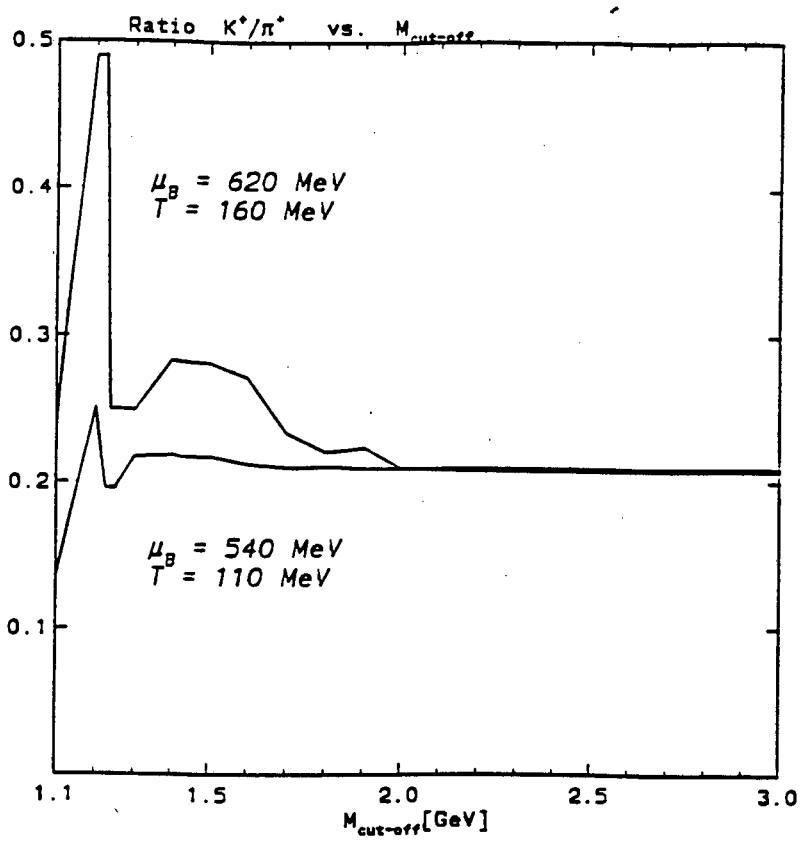

Figure 4.3: The K^+/π^+ ratio as a function of cut-off mass, at two sets of freeze-out parameters, (μ_B, T), determined in $Si - Au$ collisions at the AGS.

In [29] the baryon chemical potential is fixed by the measured pion to nucleon abundance as well as the density of the system at freeze-out. A value of $\mu_B^F = 540$ MeV is given, which we agree with. Great effort is made to avoid the variation of particle densities and density ratios at fixed rapidity. Accordingly, they integrate the experimental quantities over p_T and y, always including midrapidity, justifying the y integration on the grounds that even a rather well-localised thermal source in the centre of the colliding nuclei is spread out in y because of the width of the space-rapidity correlation, and the natural width in y of a thermal source (see Appendix E). Comparisons are then made with the Hadron Gas model theoretical values and these '4π' integrated experimental data values.

Using $\mu_B^F = 540$ MeV, two freeze-out temperatures are considered in [29], namely $T_F = 120$ MeV and $T_F = 140$ MeV, the range yielded by their method of determining the temperature. See Table (4.1) for their results.

A transverse velocity profile of $\beta_T(r) = \beta_T{}^{max}(r/R)^\alpha$ is considered in their approach to transverse flow. Accordingly the relevant equation in Appendix F becomes

$$\frac{dN}{m_T dm_T} \propto \int_0^R r dr m_T K_1\left(\frac{m_T}{T}\cosh y_T\right) I_0\left(\frac{p_T}{T}\sinh y_T\right) \tag{4.2}$$

where $y_T = tanh^{-1}(\beta_T)$. In determining the parameter $\beta_T{}^{max}$, it is found that this parameter is not very sensitive to the parameter α. A freeze-out radius of $R = 6.7$ fm is used (our freeze-out radius is $R \sim 7.5$ fm [53]). Fixing the temperature between 120 and 140 MeV,

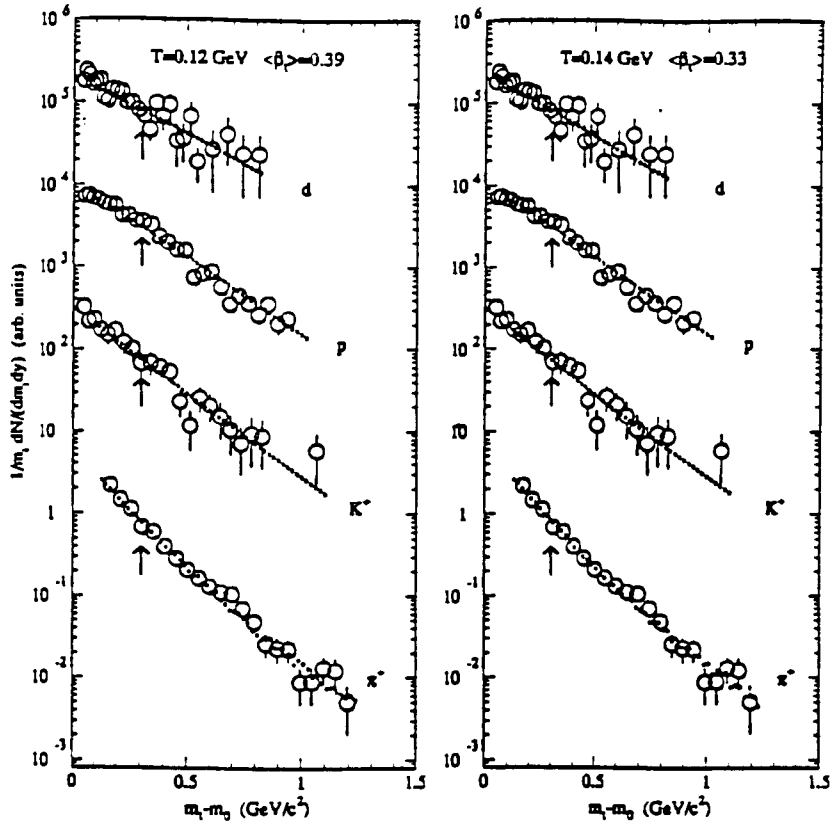

Figure 4.4: Transverse momentum spectra fitted with transverse flow for $T = 120$ MeV (left) and $T = 140$ MeV (right) for $Si - Au$ data at the AGS [29].

a single common transverse velocity to describe the data (using equation (4.2) above) is searched for. To avoid contamination of non-thermal resonances (effective for the heavier particles) they use only the data where $m_T - m_0 \geq 300$ MeV/c^2. Good agreement is found using ${\beta_T}^{max} = 0.58(0.50)$ at $T = 120(140)$ MeV (see Fig.(4.4)). This corresponds to average flow velocities of $\langle\beta_T\rangle = 0.39(0.33)$ which is calculated to imply expansion times of the order of 12 fm/c. Mention is also made of the recent azimuthal distribution of transverse energy [24] in semi-central $Au - Au$ collisions at AGS energies, in support of transverse flow in nuclear collisions. Thereafter the analysis of the $Si - Au$ data stops, and they go on to discuss quantitatively the effects of longitudinal flow on $Si - Al$ data. For completeness, I will outline those results. Using equations (2.19) and (2.20) an analysis of the rapidity spectra of $Si - Al$ (Note Al, not Au) is done, finding a suitable cutoff rapidity $\eta_{max} = 1.15$, which translates into a longitudinal flow velocity of $y_L = 0.52c$.

An earlier analysis (1990) of the $Si - Au$ data was performed using the overlapping ratios techniques by [52]. Calculated using the thermal model with vanishing overall strangeness as a constraint, the plot (shown in Fig.(4.5)) of $Si - Au$ data shows the particle ratios K^+/π^+, π^+/p and K^-/π^- having a large overlap region centred roughly on freeze-out parameters of (around)

$$T_F = 105 \pm 15 \text{ MeV} \qquad \mu_B^F = 580 \pm 60 \text{ MeV}. \tag{4.3}$$

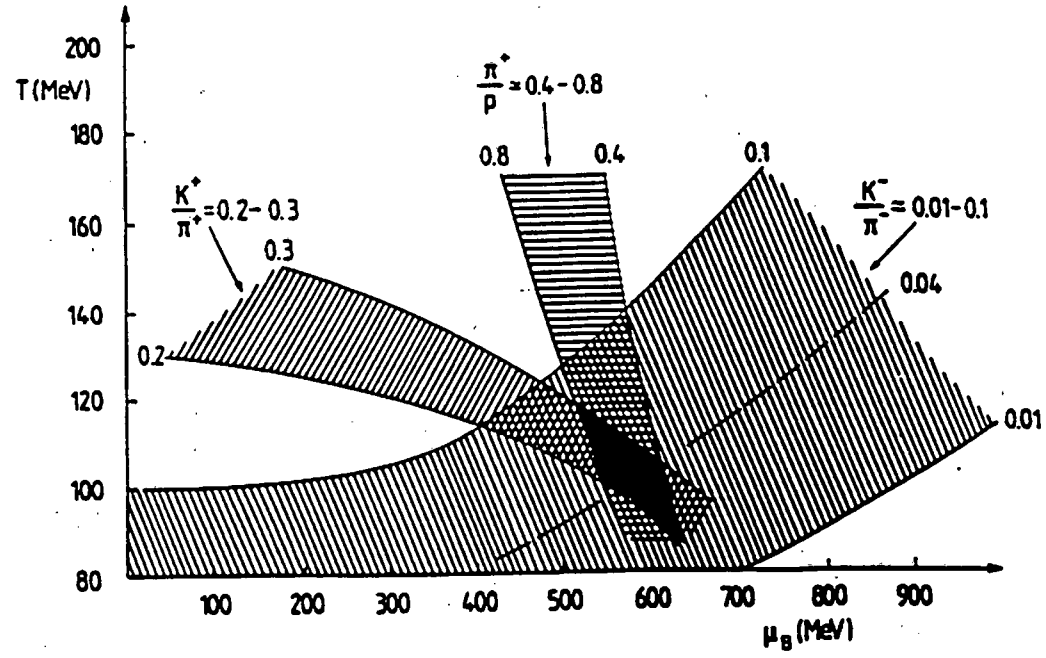

Figure 4.5: Plot of constant K^+/π^+, K^-/π^- and π^+/p ratios in the phase diagram for a hadron resonance gas in thermodynamic equilibrium [52].

prompting them to conclude that the particle ratios measured in this experiment seem to be perfectly consistent with a thermally and chemically equilibrated baryon-rich hadronic fireball, with freeze-out parameters listed above in equation (4.3). Our work is in the same vein, using the same model, only this time with the additional constraint of charge conservation and the benefit of better statistics, but their 1990 freeze-out values (eq.(4.3)) agree fairly well with ours (eq.(4.1)).

A further analysis of the $Si-Au$ data has been undertaken [54]. The Hadron Gas formalism is used, assuming only local thermal equilibration, to relate the quark-chemical potential, μ_q, and temperature, T, from a large range of experiments at SPS and AGS, including $Si-Au$. *Only* strange particle ratios (predominantly K^+/K^- and $\overline{\Lambda}/\Lambda$ ratios) are used to constrain the allowed values of μ_q/T, μ_s/T and T. This then allows them to determine the 'actual' temperature T. A further parameter is the strangeness saturation factor γ_s [55], which for $Si-Au$ they set at unity. Comparison of the inverse slope parameter of the m_T distribution with their 'actual' temperature, using equation (2.18), yields the transverse velocity v_T of the fireball. For $Si-Au$ their freeze-out parameters are

$$T_F = 140 \pm 5 \text{ MeV} \qquad \mu_B^F = 555 \pm 33 \text{ MeV}. \tag{4.4}$$

and accord a transverse flow of $v_T = 0.32 \pm 0.04c$ to the data.

These values are not very different from [29], although the temperature is a little high for

with the baryonic density n_B and baryon chemical potential μ_B. No strong conclusion is drawn, but they support [57] and find that at AGS energies the difference in pion chemical potential (40-50 MeV by their calculations) should influence pion p_T spectra, and cite data from $Au - Au$ experiments at the AGS as early tentative evidence [60].
They also predict the final freeze-out value of π^-/π^+ ratios in heavy-ion collisions, noting that this corresponds to thermal pions only. In our work [53] we have shown that the decay pions actually outgrow the thermal pions at typical AGS energies (see Fig 2.3).
Cognizance of the asymmetry of d and u quarks in heavy ion collisions was also taken by [32], and in a brief section the effect of this asymmetry is estimated. It is concluded that, although small, the difference in chemical potentials of u and d quarks is not always negilgible.

4.4 Summary.

We have here addressed the question of chemical equilibrium at freeze-out in a self-contained fashion, including the isospin asymmetry of the initial state. Our conclusion, in full agreement with [29], is that in $Si - Au$ collisions at the AGS all copiously produced hadron species are emitted in accord with their thermal weights, as calculated for an ideal gas of hadrons and hadron resonances with the freeze-out parameters given by eq.(4.1). Some less frequently produced species also agree with this. Our conclusion is thus supported by six or seven independent and directly measured hadron production ratios, so that it seems quite well-founded. In contrast, the production of the (relatively rare) antibaryons is not suppressed as much as expected in a baryon-rich environment. This agrees with results from $\bar{p}$ production in $p - A$ studies.
The freeze-out temperature determined here can in principle be counterchecked by the measured transverse momentum spectra, provided we know the expansion pattern. In the absence of any collective flow effects, we would have for light hadrons ($m_\pi \simeq 0$)

$$\langle |p_T| \rangle \simeq 2T \simeq 210 \text{ MeV}, \tag{4.6}$$

which is definitely too small. As noted in [29], this could be taken as an indication of expected flow effects [28]. However, the presence of such effects requires a more complete analysis, comparing in particular the change in transverse momentum spectra in going from $p - A$ to $A - B$ collisions.

4.5 Quo vadis Hadron Gas model.

There seems to be consensus [29, 52, 53] in the above-mentioned Hadron Gas model treatments of the the $Si - Au$ data, that at freeze-out, the hadrons are in thermal equilibrium, and most hadron species are chemically equilibrated. A recent study of the $S - Au$ data gathered at SPS reached a similar conclusion [8].

In terms of the model itself, we believe we have brought some fine tuning by ensuring overall charge conservation [53], a constraint which will be important for analyses of $Au - Au$ and $Pb - Pb$ collisions with their large asymmetry in n/p ratio ($n/p \sim 1.5$).

That the particle densities in the Hadron Gas model are defined by only two freeze-out parameters, μ_B^F and T_F is part of the model's attraction. However, a single μ_B characterising the freeze-out density of the fireball is an oversimplification, in the light of 'nuclear transparency' and rapidity distribution plots of collisions of asymmetric nuclei. The Bjorken model [7] models only the central rapidity region where it is argued that there are as many antibaryons as baryons. One step further is to model a superposition of fireballs in rapidity space. Modifying equation (2.19) we have

$$\frac{dn}{dy} = \int_{\eta_{min}}^{\eta_{max}} d\eta \frac{dn_{th}}{dy}\,(y-\eta)\rho(\eta), \tag{4.7}$$

where $\rho(\eta)$ governs the distribution of superimposed fireballs, which could have different T and μ_B, and each fireball i is given by

$$\frac{dn_{ith}}{dy} = \frac{g\lambda}{(2\pi)^3}\, m^2 T e^{\frac{-m}{T}}\, \cosh y_i \left(1 + 2\left(\frac{T}{m\cosh y_i}\right) + 2\left(\frac{T}{m\cosh y_i}\right)^2\right), \tag{4.8}$$

where $y_i = (y - y_{FB_i})$. How tractable this would prove can be speculated, but there certainly is a need to allow the baryonic density to vary within the fireball. It seems a poor approximation in the light of 'nuclear transparency' to ascribe a single μ_B to a $Si - Au$ fireball, with the two atoms being so vastly different in scale.

Table 4.1: Ratios of Hadron Species in Si-Au Collisions at the AGS [29] (Thermal parameters: $T = 120$ MeV, $T = 140$ MeV, $\mu_B = 540$ MeV).

Ratio	Thermal Model: 120 MeV	Thermal Model: 140 MeV	Experimental Ratio
$\pi/(p+n)$	1.29	1.34	1.05(5)
$d/(p+n)$	4.3×10^{-2}	5.8×10^{-2}	$3.0(3) \times 10^{-2}$
$\bar{p}/p$	1.47×10^{-4}	5.8×10^{-4}	$4.5(5) \times 10^{-4}$
K^+/π^+	2.3×10^{-1}	2.7×10^{-1}	$1.9(2) \times 10^{-1}$
K^-/π^-	5.0×10^{-2}	6.2×10^{-2}	$3.5(5) \times 10^{-2}$
$K^0{}_s/\pi^+$	1.4×10^{-1}	1.6×10^{-1}	$9.7(15) \times 10^{-2}$
K^+/K^-	4.6	4.3	4.4(4)
$\Lambda/(p+n)$	9.5×10^{-2}	1.1×10^{-1}	$8.0(16) \times 10^{-2}$
$\bar{\Lambda}/\Lambda$	8.8×10^{-4}	3.7×10^{-3}	$2.0(8) \times 10^{-3}$
$\phi/(K^+ + K^-)$	2.4×10^{-2}	3.6×10^{-2}	$1.34(36) \times 10^{-2}$
Ξ^-/Λ	6.4×10^{-2}	7.2×10^{-2}	$1.2(2) \times 10^{-1}$
$\bar{d}/\bar{p}$	1.1×10^{-5}	4.7×10^{-5}	$1.0(5) \times 10^{-5}$

for the lefthand integral, and integrating out the righthand term, replacing β with $1/T$, leaves

$$n_B = (n_q - n_{\bar{q}})/3 = [\ \mu T^2 + \mu^3/\pi^2\ ]\ /\ 18.$$

Appendix B

Cylindrical coordinates, transformation of d^3p

As discussed in the text of chapter 2, due to the cylindrical symmetry of the collision we are modelling, it is convenient to introduce two variables: y, longitudinal rapidity (which is Lorentz-additive), and m_T, transverse mass. We define y, the longitudinal rapidity, as

$$y = \tanh^{-1}\left(\frac{p_z}{E}\right).$$

We have chosen the boost to be only along the z-axis, so $p_z/E = (\beta\gamma)/\gamma = \beta$, which is just v_L as we use units where $c = 1$. Defining m_T as

$$m_T = \sqrt{m^2 + p_x^2 + p_y^2}$$

and writing the momentum 4-vector of the beam as

$$p^\mu = (E, 0, 0, p_z) = (m_T \cosh y, 0, 0, m_T \sinh y)$$

we can regain, via a few steps shown below,

$$p^\mu p_\mu = m_T^2 \cosh^2 y - m_T^2 \sinh^2 y = E^2 - p_z^2 = m_T^2,$$

the familiar relation

$$E^2 - p_x^2 - p_y^2 - p_z^2 = m^2.$$

Now we transform d^3p into cylindrical coordinates:

$$d^3p = 2\pi p_T dp_T dp_z$$

with p_T = transverse and p_z = longitudinal momenta respectively. Recognising $m_T^2 = m^2 + p_T^2$ it follows that $m_T dm_T = p_T dp_T$, which transforms the above equation into

$$d^3p = 2\pi m_T dm_T dp_z.$$

Using the definition of rapidity we have $dy = dp_z/E$, concluding the transformation of d^3p into the cylindrical coordinates y and m_T.

$$d^3p = 2\pi m_T dm_T E dy.$$

Appendix C

Derivation of the phase space terms, using Boltzmann statistics, for an ideal gas of hadrons and hadronic resonances.

If at freeze-out we have an ideal gas of hadrons and hadronic resonances, then the system is described by the partition function

$$\ln Z(T, \mu_B, \mu_S, \mu_Q) = \sum_i \lambda^i W_i.$$

Here W_i is the phase space factor for hadrons of species i. The phase space factors are given by

$$W_i = \frac{g_i m_i^2 VT}{2\pi^2} K_2\left(\frac{m_i}{T}\right),$$

with g_i denoting the spin degeneracy, m_i the mass of hadron species i; V is the volume of the system. Let us see how the above equation has come about. The Boltzmann distribution function predicts for hadron species i a particle density

$$n_i = g_i \lambda_i \int \frac{d^3p}{(2\pi)^3} e^{\frac{-E_i}{T}}$$

which, after the angle is integrated out, leaves

$$n_i = \frac{g_i \lambda_i}{2\pi^2} \int_0^\infty p^2 dp e^{\frac{-E_i}{T}}.$$

Ensuring that $p^\mu p_\mu = m^2$, we can choose our p^μ such that

$$p^\mu = (m\cosh y, 0, 0, m\sinh y),$$

where $y = \tanh^{-1}\left(\frac{p_z}{E}\right)$, which leaves

$$n_i = \frac{g_i \lambda_i}{2\pi^2} \int_0^\infty dy m_i^3 \cosh y \sinh^2 y e^{\frac{-m_i T}{T}} \cosh y.$$

Next use

$$\sinh^2 y \cosh y = \frac{1}{4}\left(\cosh 3y - \cosh y\right)$$

to reach

$$n_i = \frac{{m_i}^3 g_i \lambda_i}{8\pi^2} \int_0^\infty dy(\cosh 3y - \cosh y)\, e^{\frac{-m_i x}{T}} \cosh y.$$

Using the definition of the modified Bessel function, shown below

$$K_\nu(z) = \int_0^\infty dt \cosh(\nu(t)) e^{-z \cosh t},$$

we can rewrite it as

$$n_i = \frac{{m_i}^3 g_i \lambda_i}{8\pi^2} \left[K_3\left(\frac{m_i}{T}\right) - K_1\left(\frac{m_i}{T}\right)\right].$$

Now use $K_3(x) - K_1(x) = \left(\frac{4}{x}\right) K_2(x)$ to reach

$$\frac{n_i V}{\lambda_i} = W_i = \frac{g_i V m_i^2 T}{2\pi^2} K_2\left(\frac{m_i}{T}\right). \tag{C.1}$$

Appendix D

Derivation of equation (2.11).

Equation (2.10) reads

$$n_i = \frac{N_i}{V} = \frac{g_i}{(2\pi)^2} \; e^{\frac{\mu_i}{T}} \int_0^\infty dy \int_m^\infty dm_T m_T E e^{\frac{-m_T}{T}} \cosh y.$$

Using $E = m_T \cosh y$, equation (2.10), becomes

$$\frac{1}{{m_T}^2}\frac{dn_i}{dm_T} = \frac{g_i}{(2\pi)^2} \; e^{\frac{\mu_i}{T}} \int_0^\infty dy \cosh y e^{\frac{-m_T}{T}} \cosh y.$$

Using the definition below

$$K_\nu(z) = \int_0^\infty dt \cosh(\nu(t)) e^{-z \cosh t},$$

we can rewrite it as

$$\frac{1}{{m_T}^2}\frac{dn_i}{dm_T} = \frac{g_i}{(2\pi)^2} \; e^{\frac{\mu_i}{T}} \; K_1\left(\frac{m_T}{T}\right).$$

Appendix E

Rapidity windows and spectra.

Equation (2.13) reads

$$E\frac{d^3n}{d^3p} = \frac{g\lambda}{(2\pi)^3} m_T \cosh(y - y_{FB}) e^{\frac{-m_T}{T}} \cosh(y - y_{FB}).$$

Looking at the above equation, data which have been collected in a small rapidity window (compared with the total rapidity distribution width, say $\delta y \leq 0.5$ or so) should be compared with a thermal model by using a fit of the form

$$\frac{dn}{dydm_T} \propto m_T e^{\frac{-m_T}{T_{\text{eff}}}},$$

with $T_{\text{eff}} = T/cosh(y - y_{FB})$. In a large rapidity window around y_{FB}, the y integrated form of the above equation, in the limit where $m_T \gg T$ produces the relation

$$\frac{dn}{dm_T} \propto m_T^{\frac{3}{2}} e^{\left(\frac{-m_T}{T}\right)}.$$

Appendix F

Apparent temperature in uniform transverse flow.

At rest with the fireball, we describe its 4-velocity as:

$$u^\mu = \begin{pmatrix} 1 \\ 0 \\ 0 \\ 0 \end{pmatrix}.$$

Boosting this in the x direction, and then distributing the boost radially (i.e. only in the $x-y$ plane):

$$u^\mu = \left(\begin{pmatrix} 1 & 0 & 0 & 0 \\ 0 & \cos\phi & \sin\phi & 0 \\ 0 & \sin\phi & \cos\phi & 0 \\ 0 & 0 & 0 & 1 \end{pmatrix} \begin{pmatrix} \cosh y_T & \sinh y_T & 0 & 0 \\ \sinh y_T & \cosh y_T & 0 & 0 \\ 0 & 0 & 1 & 0 \\ 0 & 0 & 0 & 1 \end{pmatrix} \begin{pmatrix} 1 \\ 0 \\ 0 \\ 0 \end{pmatrix} \right)$$

which yields

$$u^\mu = \begin{pmatrix} \cosh y_T \\ \cos\phi \sinh y_T \\ \sin\phi \sinh y_T \\ 0 \end{pmatrix},$$

a 4-velocity describing radial flow. Evaluating the Boltzmann phase space distribution function $f(x,p) = \lambda\ e^{(-p^\mu u_\mu / T)}$ we have

$$p^\mu u_\mu = \left(\begin{pmatrix} E & p_x & p_y & p_z \end{pmatrix} \begin{pmatrix} \cosh y_T \\ -\cos\phi \sinh y_T \\ -\sin\phi \sinh y_T \\ 0 \end{pmatrix} \right),$$

resulting in $E\cosh y_T - (p_x\cos\phi + p_y \sin\phi)\sinh y_T$. Now $p_x = p_T \cos\phi_s$ and $p_y = p_T \sin\phi_s$ and, using $\cos(A-B) = \cos A \cos B - \sin A \sin B$, we get

$$p^\mu u_\mu = E\cosh y_T - p_T \cos(\phi - \phi_s)\sinh y_T.$$

Equation (2.9) can now be rewritten in the form:

$$n = \frac{g}{(2\pi)^3}\,\lambda \int_0^{2\pi} d\phi \int_0^{\infty} dy \int_{m_0}^{\infty} dm_T m_T E e^{\frac{-p^\mu u_\mu}{T}} \quad ,$$

or

$$\frac{dn}{m_T dm_T d\phi dy} = \frac{g}{(2\pi)^3}\,\lambda m_T \cosh y e^{\frac{-m_T}{T}\cosh y_T \cosh y} e^{\frac{p_T}{T}\cos(\phi-\phi_s)\sinh y_T}.$$

Integrating out the ϕ and y dependence, we recognize the $K_1\left(\frac{m_T}{T}\cosh y_T\right)$ term in the above integral, however this time it is multiplied by another term which has the form:

$$I_B(x) = \frac{1}{\pi}\int_0^{\pi} d\phi e^{x\cos\phi} e^{-iB\phi}.$$

Finally, we arrive at

$$\frac{dn}{m_T dm_T} = \frac{g}{(2\pi)^2}\,\lambda 2 m_T K_1\left(\frac{m_T}{T}\cosh y_T\right) I_0\left(\frac{p_T}{T}\sinh y_T\right). \qquad \text{(F.1)}$$

Let us look at the behaviour of the K_1 and I_0 functions when their respective arguments become very large. We see that

$$\lim_{z\to\infty} K_1(z) \sim e^{-z},$$

and

$$\lim_{z\to\infty} I_0(z) \sim e^{+z}.$$

In the limit of large p_T/T, equation F1 becomes:

$$\lim_{\frac{p_T}{T}\to\infty} K_1\left(\frac{m_T}{T}\cosh y_T\right) I_0\left(\frac{p_T}{T}\sinh y_T\right) \propto \sqrt{\frac{\pi T}{m_T\cosh y_T}}\, e^{\frac{-m_T}{T}\cosh y_T} e^{\frac{p_T}{T}\sinh y_T}.$$

Accordingly,

$$\frac{dn}{dm_T} \propto m_T^{\frac{3}{2}} e^{\frac{-m_T}{T}}\left[\cosh y_T - \sinh y_T\right]$$

or

$$\frac{dn}{dm_T} \propto m_T^{\frac{3}{2}} e^{\left(\frac{-m_T e^{y_T}}{T}\right)}.$$

Now in our boost $\cosh y_T = \gamma$ and $\sinh y_T = \beta\gamma$, allowing us to write e^{-y_T} as $\sqrt{\frac{1-\tanh y_T}{1+\tanh y_T}}$ which in turn can be expressed as $\sqrt{\frac{1-\beta}{1+\beta}}$, so

$$\frac{dn}{dm_T} \propto m_T^{\frac{3}{2}} e^{\frac{-m_T}{T}} \sqrt{\frac{1-v_T}{1+v_T}} \quad ,$$

which is compared with the expression below for a stationary fireball, hence the name 'apparent' temperature.

$$\frac{dn}{dm_T} \propto m_T^{\frac{3}{2}} e^{\left(\frac{-m_T}{T}\right)}.$$

Appendix G

Isospin-symmetric initial conditions.

In the Boltzmann approximation of an ideal gas of hadrons, the number of protons N_p is proportional to

$$N_p \propto e^{\frac{-E}{T}} e^{\frac{\mu_B}{T}} e^{\frac{\mu_Q}{T}},$$

while the number of neutrons N_n is proprtional to

$$N_n \propto e^{\frac{-E}{T}} e^{\frac{\mu_B}{T}}.$$

In isospin-symmetric initial conditions, we require $N_p = N_n$. Since their masses are virtually identical, we see that μ_Q must vanish to ensure that $N_p = N_n$.

Appendix H

The number of participants in central A - B collisions (A≪B).

The projectile A bores out a volume V_{tube} in the target B, centred on a diameter of the target, given by

$$V_{\rm tube} \simeq \pi {R_A}^2 2R_B,$$

Now $V_A = \frac{4}{3}\pi {R_A}^3 = A_A V_0$ where V_0 is the standard nucleon volume. With some manipulation, we arrive at

$${R_A}^2 = (\frac{3}{4\pi}\ A_A V_0)^{\frac{2}{3}}$$

and

$$R_B = (\frac{3}{4\pi}\ A_B V_0)^{\frac{1}{3}}\ .$$

Using the above expressions to re-express $V_{\rm tube}$.

$$V_{\rm tube} \simeq 2\pi(\frac{3}{4\pi}\ A_A V_0)^{\frac{2}{3}}\ (\frac{3}{4\pi}\ A_B V_0)^{\frac{1}{3}}$$

or

$$V_{\rm tube} \simeq \frac{3}{2}\ V_0 ({A_A}^2 B_A)^{\frac{1}{3}}\ .$$

The number of participating nucleons is given by:

$$N_{part} \simeq A_A + \frac{V_{tube}}{V_B}\ A_B.$$

Using $V_B = A_B V_0$ we reach

$$N_{part} \simeq [A + 1.5 A^{2/3} B^{1/3}].$$

Appendix I

Finite volume correction for a spherical fireball

The quantum mechanical wavefunctions that describe the spherical fireball are subject to a surface boundary condition that requires these wavefunctions to vanish at that surface. Quantitatively, we look for solutions of

$$\nabla^2\Psi + k^2\Psi = 0, \quad \Psi_{\text{surface}} = 0.$$

Each proper solution $\Psi(x,y,z) = sin(k_x x)sin(k_y y)sin(k_z z)$ corresponds to a lattice point in k space, with $k_x = l\pi/a, k_y = m\pi/a, k_z = n\pi/a$ where a is the radius of the sphere. Each state fills out a characteristic volume π^3/a^3, and the states are filled to a $\mathbf{k_{max}}$. This can be visualized as the states occupying an octant of a sphere, except for slablike regions at coordinate planes (x or y or $z = 0$), and on the shell, where the boundary condition applies. Volume = shell - correction for ring-like strips + recorrection for corners subtracted twice in counting volume of rings, or more elegantly, if we look at the number of states dN with wave no. $\mathbf{k}$ found in the interval $\mathbf{k} + d\mathbf{k}$

$$dN = \frac{Vk^2}{2\pi^2}\, d\mathbf{k} - \frac{Sk}{8\pi}\, d\mathbf{k} + \int \chi\, dS\, d\mathbf{k}/8\pi^2,$$

with V the volume, S the surface area and χ the local total curvature of the sphere, which is just L, the characteristic length of the fireball. So N, the number of allowed states with wave number less than $\mathbf{k}$

$$N = \frac{Vk^3}{6\pi^2} - \frac{Sk^2}{16\pi} + \frac{Lk}{8\pi^2}.$$

In other words, the entire geometric volume is not free to be populated by quantum states. The forbidden regions, when the volume is small, have to taken into account, hence the term 'finite volume correction'.

Appendix J

Thermodynamic consistency with excluded volumes

Beginning from a grand canonical ensemble of an ideal gas of hard sphere baryons we have, using Boltzmann statistics,

$$Z_{GC} = \sum_{N=0}^{\infty} e^{\left(\frac{\mu N}{T}\right)} \frac{1}{N!} [Z(T,V,1)]^N.$$

Performing a Laplace transformation ($\xi = P/T$) to transform the above equation into a pressure ensemble, we obtain

$$Z_P(\mu,T,P) = \int_0^{\infty} dV e^{\left(\frac{-PV}{T}\right)} \sum_{N=0}^{\infty} e^{\left(\frac{\mu N}{T}\right)} \frac{1}{N!} [Z(T,V,1)]^N.$$

Now the available volume V' is given by $V' = V - V_0 N$, where each of the N baryons in the gas has a proper or intrinsic volume of V_0, so

$$Z_P(\mu,T,P) = \sum_{N=0}^{\infty} \frac{1}{N!} [Z'(T,V',1)]^N \int_{V_0 N}^{\infty} dV (V - V_0 N)^N e^{\left(\frac{-PV}{T}\right)} e^{\left(\frac{\mu N}{T}\right)}.$$

Rewriting the integral using V' as the variable

$$Z_P(\mu,T,P) = \sum_{N=0}^{\infty} \frac{1}{N!} [Z'(T,V',1)]^N \int_0^{\infty} dV' V'^N e^{\left(\frac{-PV'}{T}\right)} e^{\left(\frac{-PNV_0}{T}\right)} e^{\left(\frac{\mu N}{T}\right)},$$

we are able to recognise the expression as the Pressure ensemble of an ideal gas with μ shifted to $\mu - PV_0$ i.e.

$$P = P_{id}(T, \mu - PV_0).$$

For calculating the baryon density we use

$$n_B = \left.\frac{\partial P}{\partial \mu}\right|_T.$$

Accordingly

$$n_B = \left.\frac{\partial P_{id}}{\partial(\mu - PV_0)}\right|_T \left.\frac{\partial(\mu - PV_0)}{\partial\mu}\right|_T,$$

or

$$n_B = \frac{\partial P_{id}}{\partial(\mu - PV_0)}\,[1 - V_0 \left.\frac{\partial P}{\partial\mu}\right|_T].$$

Denoting the density calculated for an ideal gas of pointlike baryons, each with intrinsic volume V_0, by n_B^0, we have

$$n_B = n_B^0(T, \mu - PV_0)[1 - V_0 n_B].$$

Rearranging the final expression we get

$$n_B = n_B^0[1 + V_0 n_B^0]^{-1}. \tag{J.1}$$

Note that for $\lim_{n_0\to\infty}$, $n \to 1/V_0$, the dense packing limit. In the case of several baryon species $i = 1, 2, ..., k$, equation (2) becomes

$$n_B = n_B^0[1 + \sum_{i=1}^{k} V_i n_i^0]^{-1}. \tag{J.2}$$

If each particle species has the same excluded volume then the particle ratios calculated using the 'excluded volume' ensemble are the same as those calculated in the ideal free gas of pointlike, non-interacting particles. However, if the excluded volume varies from species to species, the particle ratios are affected.

Appendix K

Particle density ratios and transverse flow.

Starting from equation (F.1) in Appendix F,

$$\frac{dN}{m_T dm_T} = \frac{gV}{(2\pi)^2}\,\lambda 2 m_T K_1\left(\frac{m_T}{T}\cosh y_T\right) I_0\left(\frac{p_T}{T}\sinh y_T\right),$$

and using $m_T dm_t = p_T dp_T$ and rearranging a little gives:

$$n \propto \int_0^\infty dp_T p_T m_T K_1\left(\frac{m_T}{T}\cosh y_T\right) I_0\left(\frac{p_T}{T}\sinh y_T\right). \tag{K.1}$$

Rescaling equation (K.1) by dividing p_T and m_T by m,

$$n \propto m^3 \int_0^\infty \frac{dp_T}{m}\frac{p_T}{m}\frac{m_T}{m} K_1\left(\frac{m_T}{mT} m\cosh y_T\right) I_0\left(\frac{p_T}{mT} m\sinh y_T\right), \tag{K.2}$$

leaving the integral dimensionless. Now, using [61], it can be shown that

$$\int_0^\infty dx\; x\sqrt{x^2+y^2} K_1\left(c\sqrt{x^2+y^2}\right) I_0(bx) = \frac{c}{(c^2-b^2)} y^2 K_2\left(y\sqrt{c^2-b^2}\right). \tag{K.3}$$

Comparing equations (K.2) and (K.3) we have

$$n \propto m^2 T \cosh y_T K_2\left(\frac{m}{T}\right). \tag{K.4}$$

The full expression for the density of particle i is thus

$$n_i = \lambda_i \frac{g_i m_i^2 T}{2\pi^2}\cosh y_T K_2\left(\frac{m_i}{T}\right). \tag{K.5}$$

Equation (K.5) is a remarkable result. Ratios of particle densities are independent of transverse flow. The phase space term of equation (K.5) differs only by a factor $\cosh y_T$ from the stationary fireball phase space term (see eq.(2.6) and Appendix C). We ascribe this to the Lorentz contraction in the transverse direction of the fireball, since $\cosh y_T = \gamma$, reducing the volume to $\gamma V_{\text{stat.}}$. This analytical proof was searched for after numerical calculations showed the ratios of particle densities to be unaffected by the inclusion of the I_0 term [25].

Appendix L

Particle Data Table.

The decay table that I compiled from [34] is listed on the following pages for completeness. In the compilation of this table I made some educated guesses where the information was incomplete. Also, one will notice that for the larger mass resonances, (typically the Δ's with masses above 2.000 GeV), often only the π decay columns are populated, violating baryon number conservation. The information for these resonances with large mass is often incomplete. I experimented with cut-off masses during the Hadron Gas calculations (see text), and found that the violation of overall baryon number was apparent when the phase space was large (a few percent for the unphysical freeze-out parameters (3.5)) when no cut-off mass was applied. At the freeze-out parameters (3.4) the effect was negligible.
I welcome a scrutiny of this table, which has fewer decay columns than the larger table which I have on disk. The particles have to recognised by their masses (in units of GeV) and charge, 'Q'. The degeneracy is denoted by 'd'.

Table L.1: Particle Decay Table listed on the following pages.

Mass	Q	d	pi+	pi-	K+	K-	p	n	lamb	alamb	sig0	asig0
0.140	+1.	1.	1.000	0.000	0.000	0.000	0.000	0.000	0.000	0.000	0.000	0.000
0.135	+0.	1.	0.000	0.000	0.000	0.000	0.000	0.000	0.000	0.000	0.000	0.000
0.140	-1.	1.	0.000	1.000	0.000	0.000	0.000	0.000	0.000	0.000	0.000	0.000
0.547	+0.	1.	0.285	0.285	0.000	0.000	0.000	0.000	0.000	0.000	0.000	0.000
0.770	+1.	3.	1.000	0.000	0.000	0.000	0.000	0.000	0.000	0.000	0.000	0.000
0.770	+0.	3.	1.000	1.000	0.000	0.000	0.000	0.000	0.000	0.000	0.000	0.000
0.770	-1.	3.	0.000	1.000	0.000	0.000	0.000	0.000	0.000	0.000	0.000	0.000
0.782	+0.	3.	0.910	0.910	0.000	0.000	0.000	0.000	0.000	0.000	0.000	0.000
0.958	+0.	1.	0.965	0.965	0.000	0.000	0.000	0.000	0.000	0.000	0.000	0.000
0.980	+0.	1.	0.521	0.521	0.110	0.110	0.000	0.000	0.000	0.000	0.000	0.000
0.982	+1.	1.	1.285	0.285	0.000	0.000	0.000	0.000	0.000	0.000	0.000	0.000
0.982	+0.	1.	0.285	0.285	0.000	0.000	0.000	0.000	0.000	0.000	0.000	0.000
0.982	-1.	1.	0.285	1.285	0.000	0.000	0.000	0.000	0.000	0.000	0.000	0.000
1.019	+0.	3.	0.157	0.157	0.491	0.491	0.000	0.000	0.000	0.000	0.000	0.000
1.170	+0.	3.	1.000	1.000	0.000	0.000	0.000	0.000	0.000	0.000	0.000	0.000
1.230	+1.	3.	1.500	0.500	0.000	0.000	0.000	0.000	0.000	0.000	0.000	0.000
1.230	+0.	3.	0.500	0.500	0.000	0.000	0.000	0.000	0.000	0.000	0.000	0.000
1.230	-1.	3.	0.500	1.500	0.000	0.000	0.000	0.000	0.000	0.000	0.000	0.000
1.231	+1.	3.	1.910	0.910	0.000	0.000	0.000	0.000	0.000	0.000	0.000	0.000
1.231	+0.	3.	0.910	0.910	0.000	0.000	0.000	0.000	0.000	0.000	0.000	0.000
1.231	-1.	3.	0.910	1.910	0.000	0.000	0.000	0.000	0.000	0.000	0.000	0.000
1.250	+0.	1.	0.624	0.624	0.038	0.038	0.000	0.000	0.000	0.000	0.000	0.000
1.275	+0.	5.	0.691	0.691	0.023	0.023	0.000	0.000	0.000	0.000	0.000	0.000
1.282	+0.	3.	1.007	1.007	0.049	0.049	0.000	0.000	0.000	0.000	0.000	0.000
1.295	+0.	1.	1.118	1.118	0.000	0.000	0.000	0.000	0.000	0.000	0.000	0.000
1.300	+1.	1.	2.000	1.000	0.000	0.000	0.000	0.000	0.000	0.000	0.000	0.000
1.300	+0.	1.	1.500	1.500	0.000	0.000	0.000	0.000	0.000	0.000	0.000	0.000
1.300	-1.	1.	1.000	2.000	0.000	0.000	0.000	0.000	0.000	0.000	0.000	0.000
1.318	+1.	5.	1.440	0.486	0.049	0.000	0.000	0.000	0.000	0.000	0.000	0.000
1.318	+0.	5.	0.836	0.836	0.025	0.025	0.000	0.000	0.000	0.000	0.000	0.000
1.318	-1.	5.	0.486	1.440	0.000	0.049	0.000	0.000	0.000	0.000	0.000	0.000
1.370	+0.	1.	1.000	1.000	0.000	0.000	0.000	0.000	0.000	0.000	0.000	0.000
1.415	+0.	3.	0.333	0.333	0.500	0.500	0.000	0.000	0.000	0.000	0.000	0.000
1.419	+0.	3.	1.000	1.000	0.000	0.000	0.000	0.000	0.000	0.000	0.000	0.000
1.420	+0.	1.	0.552	0.552	0.331	0.331	0.000	0.000	0.000	0.000	0.000	0.000
1.427	+0.	3.	0.333	0.333	0.500	0.500	0.000	0.000	0.000	0.000	0.000	0.000
1.430	+0.	5.	0.222	0.222	0.167	0.167	0.000	0.000	0.000	0.000	0.000	0.000
1.465	+1.	3.	1.000	0.000	0.000	0.000	0.000	0.000	0.000	0.000	0.000	0.000
1.465	+0.	3.	1.000	1.000	0.000	0.000	0.000	0.000	0.000	0.000	0.000	0.000
1.465	-1.	3.	0.000	1.000	0.000	0.000	0.000	0.000	0.000	0.000	0.000	0.000
1.512	+0.	3.	0.333	0.333	0.500	0.500	0.000	0.000	0.000	0.000	0.000	0.000
1.525	+0.	5.	0.159	0.159	0.356	0.356	0.000	0.000	0.000	0.000	0.000	0.000
1.581	+0.	1.	0.813	0.813	0.000	0.000	0.000	0.000	0.000	0.000	0.000	0.000
1.662	+0.	3.	1.254	1.254	0.000	0.000	0.000	0.000	0.000	0.000	0.000	0.000
1.668	+0.	7.	1.234	1.234	0.000	0.000	0.000	0.000	0.000	0.000	0.000	0.000
1.670	+1.	5.	1.498	0.598	0.058	0.028	0.000	0.000	0.000	0.000	0.000	0.000
1.670	+0.	5.	0.767	0.767	0.037	0.037	0.000	0.000	0.000	0.000	0.000	0.000
1.670	-1.	5.	0.598	1.498	0.016	0.030	0.000	0.000	0.000	0.000	0.000	0.000
1.680	+0.	1.	0.310	0.310	0.500	0.500	0.000	0.000	0.000	0.000	0.000	0.000
1.691	+1.	7.	1.901	0.835	0.044	0.010	0.000	0.000	0.000	0.000	0.000	0.000
1.691	+0.	7.	1.071	1.071	0.027	0.027	0.000	0.000	0.000	0.000	0.000	0.000
1.691	-1.	7.	0.835	1.901	0.010	0.044	0.000	0.000	0.000	0.000	0.000	0.000
1.700	+1.	3.	1.901	0.835	0.044	0.010	0.000	0.000	0.000	0.000	0.000	0.000
1.700	+0.	3.	1.071	1.071	0.027	0.027	0.000	0.000	0.000	0.000	0.000	0.000
1.700	-1.	3.	0.835	1.901	0.010	0.044	0.000	0.000	0.000	0.000	0.000	0.000
1.709	+0.	1.	0.191	0.191	0.357	0.357	0.000	0.000	0.000	0.000	0.000	0.000
1.854	+0.	7.	0.118	0.118	0.500	0.500	0.000	0.000	0.000	0.000	0.000	0.000
2.011	+0.	5.	0.313	0.313	0.982	0.982	0.000	0.000	0.000	0.000	0.000	0.000
2.044	+0.	9.	0.587	0.587	0.000	0.000	0.000	0.000	0.000	0.000	0.000	0.000
2.297	+0.	5.	0.313	0.313	0.982	0.982	0.000	0.000	0.000	0.000	0.000	0.000
2.339	+0.	5.	0.313	0.313	0.982	0.982	0.000	0.000	0.000	0.000	0.000	0.000

0.494	+1.	1.	0.000	0.000	1.000	0.000	0.000	0.000	0.000	0.000	0.000	0.000
0.498	+0.	1.	0.000	0.000	0.000	0.000	0.000	0.000	0.000	0.000	0.000	0.000
0.892	+1.	3.	0.667	0.000	0.333	0.000	0.000	0.000	0.000	0.000	0.000	0.000
0.896	+0.	3.	0.000	0.667	0.667	0.000	0.000	0.000	0.000	0.000	0.000	0.000
1.273	+1.	3.	0.926	0.446	0.515	0.001	0.000	0.000	0.000	0.000	0.000	0.000
1.273	+0.	3.	0.446	0.926	0.468	0.001	0.000	0.000	0.000	0.000	0.000	0.000
1.402	+1.	3.	0.887	0.449	0.563	0.001	0.000	0.000	0.000	0.000	0.000	0.000
1.402	+0.	3.	0.449	0.887	0.439	0.001	0.000	0.000	0.000	0.000	0.000	0.000
1.412	+1.	3.	0.880	0.410	0.530	0.000	0.000	0.000	0.000	0.000	0.000	0.000
1.412	+0.	3.	0.410	0.880	0.470	0.000	0.000	0.000	0.000	0.000	0.000	0.000
1.429	+1.	1.	0.620	0.000	0.310	0.000	0.000	0.000	0.000	0.000	0.000	0.000
1.429	+0.	1.	0.000	0.620	0.620	0.000	0.000	0.000	0.000	0.000	0.000	0.000
1.425	+1.	5.	0.828	0.269	0.436	0.000	0.000	0.000	0.000	0.000	0.000	0.000
1.432	+0.	5.	0.269	0.828	0.560	0.000	0.000	0.000	0.000	0.000	0.000	0.000
1.714	+1.	3.	0.838	0.238	0.400	0.000	0.000	0.000	0.000	0.000	0.000	0.000
1.714	+0.	3.	0.238	0.838	0.600	0.000	0.000	0.000	0.000	0.000	0.000	0.000
1.773	+1.	5.	0.873	0.413	0.517	0.000	0.000	0.000	0.000	0.000	0.000	0.000
1.773	+0.	5.	0.413	0.873	0.483	0.000	0.000	0.000	0.000	0.000	0.000	0.000
1.770	+1.	7.	0.844	0.294	0.446	0.000	0.000	0.000	0.000	0.000	0.000	0.000
1.770	+0.	7.	0.294	0.844	0.550	0.000	0.000	0.000	0.000	0.000	0.000	0.000
2.045	+1.	9.	0.491	0.231	0.189	0.021	0.000	0.000	0.000	0.000	0.000	0.000
2.045	+0.	9.	0.231	0.491	0.257	0.021	0.000	0.000	0.000	0.000	0.000	0.000
0.498	+0.	1.	0.000	0.000	0.000	0.000	0.000	0.000	0.000	0.000	0.000	0.000
0.494	-1.	1.	0.000	0.000	0.000	1.000	0.000	0.000	0.000	0.000	0.000	0.000
0.896	+0.	3.	0.667	0.000	0.000	0.667	0.000	0.000	0.000	0.000	0.000	0.000
0.892	-1.	3.	0.000	0.667	0.000	0.333	0.000	0.000	0.000	0.000	0.000	0.000
1.273	+0.	3.	0.926	0.446	0.001	0.468	0.000	0.000	0.000	0.000	0.000	0.000
1.273	-1.	3.	0.446	0.926	0.001	0.515	0.000	0.000	0.000	0.000	0.000	0.000
1.402	+0.	3.	0.887	0.449	0.001	0.439	0.000	0.000	0.000	0.000	0.000	0.000
1.402	-1.	3.	0.449	0.887	0.001	0.563	0.000	0.000	0.000	0.000	0.000	0.000
1.412	+0.	3.	0.880	0.410	0.000	0.470	0.000	0.000	0.000	0.000	0.000	0.000
1.412	-1.	3.	0.410	0.880	0.000	0.530	0.000	0.000	0.000	0.000	0.000	0.000
1.429	+0.	1.	0.620	0.000	0.000	0.620	0.000	0.000	0.000	0.000	0.000	0.000
1.429	-1.	1.	0.000	0.620	0.000	0.310	0.000	0.000	0.000	0.000	0.000	0.000
1.432	+0.	5.	0.828	0.269	0.000	0.560	0.000	0.000	0.000	0.000	0.000	0.000
1.425	-1.	5.	0.269	0.828	0.000	0.436	0.000	0.000	0.000	0.000	0.000	0.000
1.714	+0.	3.	0.838	0.238	0.000	0.600	0.000	0.000	0.000	0.000	0.000	0.000
1.714	-1.	3.	0.238	0.838	0.000	0.400	0.000	0.000	0.000	0.000	0.000	0.000
1.773	+0.	5.	0.873	0.413	0.000	0.483	0.000	0.000	0.000	0.000	0.000	0.000
1.773	-1.	5.	0.413	0.873	0.000	0.517	0.000	0.000	0.000	0.000	0.000	0.000
1.770	+0.	7.	0.844	0.294	0.000	0.550	0.000	0.000	0.000	0.000	0.000	0.000
1.770	-1.	7.	0.294	0.844	0.000	0.446	0.000	0.000	0.000	0.000	0.000	0.000
2.045	+0.	9.	0.491	0.231	0.021	0.257	0.000	0.000	0.000	0.000	0.000	0.000
2.045	-1.	9.	0.231	0.491	0.021	0.189	0.000	0.000	0.000	0.000	0.000	0.000
0.938	+1.	2.	0.000	0.000	0.000	0.000	1.000	0.000	0.000	0.000	0.000	0.000
0.940	+0.	2.	0.000	0.000	0.000	0.000	0.000	1.000	0.000	0.000	0.000	0.000
1.440	+1.	2.	0.661	0.072	0.000	0.000	0.494	0.506	0.000	0.000	0.000	0.000
1.440	+0.	2.	0.072	0.661	0.000	0.000	0.506	0.494	0.000	0.000	0.000	0.000
1.520	+1.	4.	0.722	0.111	0.000	0.000	0.456	0.544	0.000	0.000	0.000	0.000
1.520	+0.	4.	0.111	0.722	0.000	0.000	0.544	0.456	0.000	0.000	0.000	0.000
1.535	+1.	2.	0.506	0.152	0.000	0.000	0.645	0.355	0.000	0.000	0.000	0.000
1.535	+0.	2.	0.152	0.506	0.000	0.000	0.355	0.645	0.000	0.000	0.000	0.000
1.650	+1.	2.	0.648	0.032	0.070	0.000	0.328	0.602	0.070	0.000	0.000	0.000
1.650	+0.	2.	0.032	0.648	0.000	0.000	0.602	0.328	0.070	0.000	0.000	0.000
1.675	+1.	6.	0.636	0.031	0.000	0.000	0.578	0.422	0.000	0.000	0.000	0.000
1.675	+0.	6.	0.031	0.636	0.000	0.000	0.422	0.578	0.000	0.000	0.000	0.000
1.680	+1.	6.	0.691	0.142	0.000	0.000	0.484	0.516	0.000	0.000	0.000	0.000
1.680	+0.	6.	0.142	0.691	0.000	0.000	0.516	0.484	0.000	0.000	0.000	0.000
1.700	+1.	4.	0.714	0.119	0.000	0.000	0.622	0.378	0.000	0.000	0.000	0.000
1.700	+0.	4.	0.119	0.714	0.000	0.000	0.378	0.622	0.000	0.000	0.000	0.000
1.710	+1.	2.	0.600	0.233	0.150	0.000	0.583	0.267	0.150	0.000	0.000	0.000
1.710	+0.	2.	0.233	0.600	0.000	0.000	0.267	0.583	0.150	0.000	0.000	0.000
1.720	+1.	4.	0.870	0.257	0.080	0.000	0.307	0.613	0.080	0.000	0.000	0.000
1.720	+0.	4.	0.257	0.870	0.000	0.000	0.613	0.307	0.080	0.000	0.000	0.000

1.900	+1.	4.	0.913	0.247	0.000	0.000	0.333	0.667	0.000	0.000	0.000	0.000
1.900	+0.	4.	0.247	0.913	0.000	0.000	0.667	0.333	0.000	0.000	0.000	0.000
1.990	+1.	8.	0.049	0.009	0.000	0.000	0.050	0.040	0.000	0.000	0.000	0.000
1.990	+0.	8.	0.009	0.049	0.000	0.000	0.040	0.050	0.000	0.000	0.000	0.000
2.000	+1.	6.	0.902	0.263	0.007	0.000	0.398	0.595	0.000	0.000	0.007	0.000
2.000	+0.	6.	0.263	0.902	0.013	0.000	0.589	0.411	0.000	0.000	0.007	0.000
2.080	+1.	4.	0.621	0.310	0.010	0.000	0.796	0.184	0.010	0.000	0.000	0.000
2.080	+0.	4.	0.310	0.621	0.000	0.000	0.184	0.796	0.010	0.000	0.000	0.000
2.090	+1.	2.	0.080	0.000	0.000	0.000	0.040	0.080	0.000	0.000	0.000	0.000
2.090	+0.	2.	0.000	0.080	0.000	0.000	0.080	0.040	0.000	0.000	0.000	0.000
2.100	+1.	2.	0.247	0.013	0.000	0.000	0.237	0.153	0.000	0.000	0.000	0.000
2.100	+0.	2.	0.013	0.247	0.000	0.000	0.153	0.237	0.000	0.000	0.000	0.000
2.190	+1.	8.	0.526	0.146	0.000	0.000	0.210	0.380	0.000	0.000	0.000	0.000
2.190	+0.	8.	0.146	0.526	0.000	0.000	0.380	0.210	0.000	0.000	0.000	0.000
2.200	+1.	6.	0.074	0.014	0.020	0.000	0.080	0.060	0.020	0.000	0.000	0.000
2.200	+0.	6.	0.014	0.074	0.000	0.000	0.060	0.080	0.020	0.000	0.000	0.000
2.220	+1.	10.	0.100	0.000	0.000	0.000	0.050	0.100	0.000	0.000	0.000	0.000
2.220	+0.	10.	0.000	0.100	0.000	0.000	0.100	0.050	0.000	0.000	0.000	0.000
2.250	+1.	10.	0.067	0.000	0.000	0.000	0.033	0.067	0.000	0.000	0.000	0.000
2.250	+0.	10.	0.000	0.067	0.000	0.000	0.067	0.033	0.000	0.000	0.000	0.000
2.600	+1.	12.	0.050	0.000	0.000	0.000	0.025	0.050	0.000	0.000	0.000	0.000
2.600	+0.	12.	0.000	0.050	0.000	0.000	0.050	0.025	0.000	0.000	0.000	0.000
2.700	+1.	14.	0.033	0.000	0.000	0.000	0.017	0.033	0.000	0.000	0.000	0.000
2.700	+0.	14.	0.000	0.033	0.000	0.000	0.033	0.017	0.000	0.000	0.000	0.000
1.232	+2.	4.	0.995	0.000	0.000	0.000	0.995	0.000	0.000	0.000	0.000	0.000
1.232	+1.	4.	0.332	0.000	0.000	0.000	0.663	0.332	0.000	0.000	0.000	0.000
1.232	+0.	4.	0.000	0.332	0.000	0.000	0.332	0.663	0.000	0.000	0.000	0.000
1.232	-1.	4.	0.000	0.995	0.000	0.000	0.000	0.995	0.000	0.000	0.000	0.000
1.600	+2.	4.	1.204	0.014	0.000	0.000	0.823	0.174	0.000	0.000	0.000	0.000
1.600	+1.	4.	0.834	0.438	0.000	0.000	0.607	0.390	0.000	0.000	0.000	0.000
1.600	+0.	4.	0.438	0.834	0.000	0.000	0.390	0.607	0.000	0.000	0.000	0.000
1.600	-1.	4.	0.014	1.204	0.000	0.000	0.174	0.823	0.000	0.000	0.000	0.000
1.620	+2.	2.	1.077	0.000	0.000	0.000	0.919	0.078	0.000	0.000	0.000	0.000
1.620	+1.	2.	0.806	0.447	0.000	0.000	0.639	0.358	0.000	0.000	0.000	0.000
1.620	+0.	2.	0.447	0.806	0.000	0.000	0.358	0.639	0.000	0.000	0.000	0.000
1.620	-1.	2.	0.000	1.077	0.000	0.000	0.078	0.919	0.000	0.000	0.000	0.000
1.700	+2.	4.	1.057	0.000	0.000	0.000	0.939	0.058	0.000	0.000	0.000	0.000
1.700	+1.	4.	0.880	0.527	0.000	0.000	0.646	0.352	0.000	0.000	0.000	0.000
1.700	+0.	4.	0.527	0.880	0.000	0.000	0.352	0.646	0.000	0.000	0.000	0.000
1.700	-1.	4.	0.000	1.057	0.000	0.000	0.058	0.939	0.000	0.000	0.000	0.000
1.750	+2.	2.	0.545	0.020	0.000	0.000	0.218	0.142	0.000	0.000	0.000	0.000
1.750	+1.	2.	0.250	0.075	0.000	0.000	0.193	0.167	0.000	0.000	0.000	0.000
1.750	+0.	2.	0.075	0.250	0.000	0.000	0.167	0.193	0.000	0.000	0.000	0.000
1.750	-1.	2.	0.020	0.545	0.000	0.000	0.142	0.218	0.000	0.000	0.000	0.000
1.900	+2.	2.	1.059	0.004	0.000	0.000	0.947	0.052	0.000	0.000	0.000	0.000
1.900	+1.	2.	0.847	0.496	0.000	0.000	0.649	0.350	0.000	0.000	0.000	0.000
1.900	+0.	2.	0.496	0.847	0.000	0.000	0.350	0.649	0.000	0.000	0.000	0.000
1.900	-1.	2.	0.004	1.059	0.000	0.000	0.052	0.947	0.000	0.000	0.000	0.000
1.905	+2.	6.	1.026	0.000	0.000	0.000	0.972	0.027	0.000	0.000	0.000	0.000
1.905	+1.	6.	0.924	0.496	0.000	0.000	0.657	0.342	0.000	0.000	0.000	0.000
1.905	+0.	6.	0.496	0.924	0.000	0.000	0.342	0.657	0.000	0.000	0.000	0.000
1.905	-1.	6.	0.000	1.026	0.000	0.000	0.027	0.972	0.000	0.000	0.000	0.000
1.910	+2.	2.	1.347	0.038	0.000	0.000	0.734	0.266	0.000	0.000	0.000	0.000
1.910	+1.	2.	0.744	0.307	0.000	0.000	0.578	0.422	0.000	0.000	0.000	0.000
1.910	+0.	2.	0.307	0.744	0.000	0.000	0.422	0.578	0.000	0.000	0.000	0.000
1.910	-1.	2.	0.038	1.347	0.000	0.000	0.266	0.734	0.000	0.000	0.000	0.000
1.920	+2.	4.	1.260	0.020	0.000	0.000	0.778	0.219	0.000	0.000	0.000	0.000
1.920	+1.	4.	0.833	0.420	0.000	0.000	0.592	0.405	0.000	0.000	0.000	0.000
1.920	+0.	4.	0.420	0.833	0.000	0.000	0.405	0.592	0.000	0.000	0.000	0.000
1.920	-1.	4.	0.020	1.260	0.000	0.000	0.219	0.778	0.000	0.000	0.000	0.000
1.930	+2.	6.	0.150	0.000	0.000	0.000	0.150	0.000	0.000	0.000	0.000	0.000
1.930	+1.	6.	0.050	0.000	0.000	0.000	0.100	0.050	0.000	0.000	0.000	0.000
1.930	+0.	6.	0.000	0.050	0.000	0.000	0.050	0.100	0.000	0.000	0.000	0.000
1.930	-1.	6.	0.000	0.150	0.000	0.000	0.000	0.150	0.000	0.000	0.000	0.000

1.940	+2.	4.	1.061	0.000	0.000	0.000	0.935	0.062	0.000	0.000	0.000	0.000
1.940	+1.	4.	0.858	0.505	0.000	0.000	0.644	0.353	0.000	0.000	0.000	0.000
1.940	+0.	4.	0.505	0.858	0.000	0.000	0.353	0.644	0.000	0.000	0.000	0.000
1.940	-1.	4.	0.000	1.061	0.000	0.000	0.062	0.935	0.000	0.000	0.000	0.000
1.950	+2.	8.	0.839	0.000	0.000	0.000	0.759	0.040	0.000	0.000	0.000	0.000
1.950	+1.	8.	0.519	0.240	0.000	0.000	0.519	0.280	0.000	0.000	0.000	0.000
1.950	+0.	8.	0.240	0.519	0.000	0.000	0.280	0.519	0.000	0.000	0.000	0.000
1.950	-1.	8.	0.000	0.839	0.000	0.000	0.040	0.759	0.000	0.000	0.000	0.000
2.000	+2.	6.	1.097	0.000	0.000	0.000	0.897	0.100	0.000	0.000	0.000	0.000
2.000	+1.	6.	0.965	0.448	0.000	0.000	0.631	0.365	0.000	0.000	0.000	0.000
2.000	+0.	6.	0.448	0.965	0.000	0.000	0.365	0.631	0.000	0.000	0.000	0.000
2.000	-1.	6.	0.000	1.097	0.000	0.000	0.100	0.897	0.000	0.000	0.000	0.000
2.150	+2.	2.	0.100	0.000	0.000	0.000	0.100	0.000	0.000	0.000	0.000	0.000
2.150	+1.	2.	0.033	0.000	0.000	0.000	0.067	0.033	0.000	0.000	0.000	0.000
2.150	+0.	2.	0.000	0.033	0.000	0.000	0.033	0.067	0.000	0.000	0.000	0.000
2.150	-1.	2.	0.000	0.100	0.000	0.000	0.000	0.100	0.000	0.000	0.000	0.000
2.200	+2.	8.	0.070	0.000	0.000	0.000	0.070	0.000	0.000	0.000	0.000	0.000
2.200	+1.	8.	0.023	0.000	0.000	0.000	0.047	0.023	0.000	0.000	0.000	0.000
2.200	+0.	8.	0.000	0.023	0.000	0.000	0.023	0.047	0.000	0.000	0.000	0.000
2.200	-1.	8.	0.000	0.070	0.000	0.000	0.000	0.070	0.000	0.000	0.000	0.000
2.300	+2.	10.	0.050	0.000	0.000	0.000	0.050	0.000	0.000	0.000	0.000	0.000
2.300	+1.	10.	0.017	0.000	0.000	0.000	0.033	0.017	0.000	0.000	0.000	0.000
2.300	+0.	10.	0.000	0.017	0.000	0.000	0.017	0.033	0.000	0.000	0.000	0.000
2.300	-1.	10.	0.000	0.050	0.000	0.000	0.000	0.050	0.000	0.000	0.000	0.000
2.350	+2.	6.	0.050	0.000	0.000	0.000	0.050	0.000	0.000	0.000	0.000	0.000
2.350	+1.	6.	0.017	0.000	0.000	0.000	0.033	0.017	0.000	0.000	0.000	0.000
2.350	+0.	6.	0.000	0.017	0.000	0.000	0.017	0.033	0.000	0.000	0.000	0.000
2.350	-1.	6.	0.000	0.050	0.000	0.000	0.000	0.050	0.000	0.000	0.000	0.000
2.390	+2.	8.	0.080	0.000	0.000	0.000	0.080	0.000	0.000	0.000	0.000	0.000
2.390	+1.	8.	0.027	0.000	0.000	0.000	0.053	0.027	0.000	0.000	0.000	0.000
2.390	+0.	8.	0.000	0.027	0.000	0.000	0.027	0.053	0.000	0.000	0.000	0.000
2.390	-1.	8.	0.000	0.080	0.000	0.000	0.000	0.080	0.000	0.000	0.000	0.000
2.400	+2.	10.	0.070	0.000	0.000	0.000	0.070	0.000	0.000	0.000	0.000	0.000
2.400	+1.	10.	0.023	0.000	0.000	0.000	0.047	0.023	0.000	0.000	0.000	0.000
2.400	+0.	10.	0.000	0.023	0.000	0.000	0.023	0.047	0.000	0.000	0.000	0.000
2.400	-1.	10.	0.000	0.070	0.000	0.000	0.000	0.070	0.000	0.000	0.000	0.000
2.420	+2.	12.	0.100	0.000	0.000	0.000	0.100	0.000	0.000	0.000	0.000	0.000
2.420	+1.	12.	0.033	0.000	0.000	0.000	0.067	0.033	0.000	0.000	0.000	0.000
2.420	+0.	12.	0.000	0.033	0.000	0.000	0.033	0.067	0.000	0.000	0.000	0.000
2.420	-1.	12.	0.000	0.100	0.000	0.000	0.000	0.100	0.000	0.000	0.000	0.000
2.750	+2.	14.	0.050	0.000	0.000	0.000	0.050	0.000	0.000	0.000	0.000	0.000
2.750	+1.	14.	0.017	0.000	0.000	0.000	0.033	0.017	0.000	0.000	0.000	0.000
2.750	+0.	14.	0.000	0.017	0.000	0.000	0.017	0.033	0.000	0.000	0.000	0.000
2.750	-1.	14.	0.000	0.050	0.000	0.000	0.000	0.050	0.000	0.000	0.000	0.000
2.950	+2.	16.	0.040	0.000	0.000	0.000	0.040	0.000	0.000	0.000	0.000	0.000
2.950	+1.	16.	0.013	0.000	0.000	0.000	0.027	0.013	0.000	0.000	0.000	0.000
2.950	+0.	16.	0.000	0.013	0.000	0.000	0.013	0.027	0.000	0.000	0.000	0.000
2.950	-1.	16.	0.000	0.040	0.000	0.000	0.000	0.040	0.000	0.000	0.000	0.000
1.116	+0.	2.	0.000	0.000	0.000	0.000	0.000	0.000	1.000	0.000	0.000	0.000
1.405	+0.	2.	0.494	0.666	0.000	0.000	0.172	0.494	0.000	0.000	0.333	0.000
1.520	+0.	4.	0.281	0.357	0.000	0.224	0.300	0.442	0.092	0.000	0.167	0.000
1.600	+0.	2.	0.173	0.233	0.000	0.113	0.173	0.285	0.000	0.000	0.117	0.000
1.670	+0.	2.	0.372	0.444	0.000	0.100	0.172	0.306	0.382	0.000	0.139	0.000
1.690	+0.	4.	0.481	0.566	0.000	0.125	0.211	0.372	0.250	0.000	0.167	0.000
1.800	+0.	2.	0.060	0.064	0.000	0.218	0.178	0.250	0.009	0.000	0.007	0.000
1.810	+0.	2.	0.249	0.283	0.000	0.325	0.434	0.499	0.000	0.000	0.067	0.000
1.820	+0.	6.	0.110	0.131	0.000	0.300	0.320	0.359	0.081	0.000	0.040	0.000
1.830	+0.	6.	0.417	0.516	0.000	0.035	0.134	0.318	0.206	0.000	0.183	0.000
1.890	+0.	4.	0.082	0.096	0.000	0.147	0.163	0.188	0.053	0.000	0.026	0.000
2.020	+0.	8.	0.250	0.327	0.000	0.025	0.102	0.247	0.030	0.000	0.150	0.000
2.100	+0.	8.	0.120	0.129	0.000	0.200	0.234	0.250	0.050	0.000	0.017	0.000
2.110	+0.	6.	0.288	0.332	0.000	0.192	0.294	0.375	0.056	0.000	0.085	0.000
2.325	+0.	4.	0.018	0.018	0.000	0.100	0.100	0.100	0.020	0.000	0.000	0.000
2.350	+0.	10.	0.068	0.085	0.000	0.060	0.077	0.109	0.020	0.000	0.033	0.000

1.189	+1.	2.	0.483	0.000	0.000	0.000	0.516	0.483	0.000	0.000	0.000	0.000
1.193	+0.	2.	0.000	0.000	0.000	0.000	0.000	0.000	0.000	0.000	1.000	0.000
1.197	-1.	2.	0.000	0.998	0.000	0.000	0.000	0.998	0.000	0.000	0.000	0.000
1.383	+1.	4.	0.967	0.000	0.000	0.000	0.031	0.029	0.880	0.000	0.060	0.000
1.384	+0.	4.	0.089	0.120	0.000	0.000	0.031	0.089	0.880	0.000	0.000	0.000
1.387	-1.	4.	0.000	1.000	0.000	0.000	0.000	0.060	0.880	0.000	0.060	0.000
1.660	+1.	2.	0.133	0.000	0.000	0.000	0.222	0.021	0.070	0.000	0.043	0.000
1.660	+0.	2.	0.063	0.085	0.000	0.100	0.122	0.163	0.070	0.000	0.000	0.000
1.660	-1.	2.	0.000	0.155	0.000	0.200	0.000	0.242	0.070	0.000	0.043	0.000
1.670	+1.	4.	0.434	0.000	0.000	0.000	0.216	0.109	0.100	0.000	0.225	0.000
1.670	+0.	4.	0.334	0.450	0.000	0.050	0.166	0.383	0.100	0.000	0.000	0.000
1.670	-1.	4.	0.000	0.550	0.000	0.100	0.000	0.325	0.100	0.000	0.225	0.000
1.750	+1.	2.	0.439	0.108	0.000	0.000	0.448	0.189	0.114	0.000	0.029	0.000
1.750	+0.	2.	0.265	0.278	0.000	0.125	0.140	0.168	0.114	0.000	0.358	0.000
1.750	-1.	2.	0.105	0.637	0.000	0.250	0.002	0.634	0.100	0.000	0.029	0.000
1.775	+1.	6.	0.559	0.077	0.000	0.000	0.473	0.104	0.276	0.000	0.056	0.000
1.775	+0.	6.	0.184	0.211	0.000	0.200	0.272	0.322	0.276	0.000	0.039	0.000
1.775	-1.	6.	0.061	0.587	0.000	0.400	0.062	0.516	0.276	0.000	0.056	0.000
1.915	+1.	6.	0.316	0.001	0.000	0.000	0.175	0.082	0.098	0.000	0.146	0.000
1.915	+0.	6.	0.235	0.310	0.000	0.050	0.125	0.266	0.098	0.000	0.001	0.000
1.915	-1.	6.	0.001	0.391	0.000	0.100	0.000	0.246	0.098	0.000	0.146	0.000
1.940	+1.	4.	0.711	0.092	0.000	0.252	0.381	0.158	0.107	0.000	0.103	0.000
1.940	+0.	4.	0.267	0.317	0.000	0.241	0.291	0.386	0.107	0.000	0.045	0.000
1.940	-1.	4.	0.072	0.763	0.000	0.230	0.159	0.527	0.107	0.000	0.103	0.000
2.030	+1.	8.	0.730	0.064	0.000	0.183	0.478	0.110	0.332	0.000	0.070	0.000
2.030	+0.	8.	0.252	0.287	0.000	0.246	0.280	0.344	0.332	0.000	0.033	0.000
2.030	-1.	8.	0.050	0.793	0.000	0.310	0.063	0.525	0.332	0.000	0.070	0.000
2.070	+1.	6.	0.111	0.000	0.000	0.000	0.119	0.036	0.000	0.000	0.075	0.000
2.070	+0.	6.	0.111	0.150	0.000	0.040	0.119	0.151	0.000	0.000	0.000	0.000
2.070	-1.	6.	0.000	0.150	0.000	0.080	0.000	0.155	0.000	0.000	0.075	0.000
1.315	+0.	2.	0.000	0.000	0.000	0.000	0.000	0.000	0.000	0.000	0.000	0.000
1.321	-1.	2.	0.000	0.000	0.000	0.000	0.000	0.000	0.000	0.000	0.000	0.000
1.532	+0.	4.	0.667	0.000	0.000	0.000	0.000	0.000	0.000	0.000	0.000	0.000
1.535	-1.	4.	0.000	0.667	0.000	0.000	0.000	0.000	0.000	0.000	0.000	0.000
1.823	+0.	4.	0.222	0.111	0.000	0.000	0.000	0.000	0.500	0.000	0.000	0.000
1.823	-1.	4.	0.111	0.222	0.000	0.500	0.000	0.000	0.500	0.000	0.000	0.000
2.025	+0.	6.	0.258	0.000	0.000	0.533	0.000	0.000	0.200	0.000	0.267	0.000
2.025	-1.	6.	0.000	0.258	0.000	0.267	0.000	0.000	0.200	0.000	0.267	0.000
1.672	-1.	4.	0.000	0.236	0.000	0.678	0.000	0.000	0.678	0.000	0.000	0.000
0.938	-1.	2.	0.000	0.000	0.000	0.000	0.000	0.000	0.000	0.000	0.000	0.000
0.940	+0.	2.	0.000	0.000	0.000	0.000	0.000	0.000	0.000	0.000	0.000	0.000
1.440	-1.	2.	0.072	0.661	0.000	0.000	0.000	0.000	0.000	0.000	0.000	0.000
1.440	+0.	2.	0.661	0.072	0.000	0.000	0.000	0.000	0.000	0.000	0.000	0.000
1.520	-1.	4.	0.111	0.722	0.000	0.000	0.000	0.000	0.000	0.000	0.000	0.000
1.520	+0.	4.	0.722	0.111	0.000	0.000	0.000	0.000	0.000	0.000	0.000	0.000
1.535	-1.	2.	0.152	0.506	0.000	0.000	0.000	0.000	0.000	0.000	0.000	0.000
1.535	+0.	2.	0.506	0.152	0.000	0.000	0.000	0.000	0.000	0.000	0.000	0.000
1.650	-1.	2.	0.032	0.648	0.000	0.070	0.000	0.000	0.000	0.070	0.000	0.000
1.650	+0.	2.	0.648	0.032	0.000	0.000	0.000	0.000	0.000	0.070	0.000	0.000
1.675	-1.	6.	0.031	0.636	0.000	0.000	0.000	0.000	0.000	0.000	0.000	0.000
1.675	+0.	6.	0.636	0.031	0.000	0.000	0.000	0.000	0.000	0.000	0.000	0.000
1.680	-1.	6.	0.142	0.691	0.000	0.000	0.000	0.000	0.000	0.000	0.000	0.000
1.680	+0.	6.	0.691	0.142	0.000	0.000	0.000	0.000	0.000	0.000	0.000	0.000
1.700	-1.	4.	0.119	0.714	0.000	0.000	0.000	0.000	0.000	0.000	0.000	0.000
1.700	+0.	4.	0.714	0.119	0.000	0.000	0.000	0.000	0.000	0.000	0.000	0.000
1.710	-1.	2.	0.233	0.600	0.000	0.150	0.000	0.000	0.000	0.150	0.000	0.000
1.710	+0.	2.	0.600	0.233	0.000	0.000	0.000	0.000	0.000	0.150	0.000	0.000
1.720	-1.	4.	0.257	0.870	0.000	0.080	0.000	0.000	0.000	0.080	0.000	0.000
1.720	+0.	4.	0.870	0.257	0.000	0.000	0.000	0.000	0.000	0.080	0.000	0.000
1.900	-1.	4.	0.247	0.913	0.000	0.000	0.000	0.000	0.000	0.000	0.000	0.000
1.900	+0.	4.	0.913	0.247	0.000	0.000	0.000	0.000	0.000	0.000	0.000	0.000
1.990	-1.	8.	0.009	0.049	0.000	0.000	0.000	0.000	0.000	0.000	0.000	0.000
1.990	+0.	8.	0.049	0.009	0.000	0.000	0.000	0.000	0.000	0.000	0.000	0.000
2.000	-1.	6.	0.263	0.902	0.000	0.007	0.000	0.000	0.000	0.000	0.000	0.007

2.000	+0.	6.	0.902	0.263	0.000	0.013	0.000	0.000	0.000	0.000	0.000	0.007
2.080	-1.	4.	0.310	0.621	0.000	0.010	0.000	0.000	0.000	0.010	0.000	0.000
2.080	+0.	4.	0.621	0.310	0.000	0.000	0.000	0.000	0.000	0.010	0.000	0.000
2.090	-1.	2.	0.000	0.080	0.000	0.000	0.000	0.000	0.000	0.000	0.000	0.000
2.090	+0.	2.	0.080	0.000	0.000	0.000	0.000	0.000	0.000	0.000	0.000	0.000
2.100	-1.	2.	0.013	0.247	0.000	0.000	0.000	0.000	0.000	0.000	0.000	0.000
2.100	+0.	2.	0.247	0.013	0.000	0.000	0.000	0.000	0.000	0.000	0.000	0.000
2.190	-1.	8.	0.146	0.526	0.000	0.000	0.000	0.000	0.000	0.000	0.000	0.000
2.190	+0.	8.	0.526	0.146	0.000	0.000	0.000	0.000	0.000	0.000	0.000	0.000
2.200	-1.	6.	0.014	0.074	0.000	0.020	0.000	0.000	0.000	0.020	0.000	0.000
2.200	+0.	6.	0.074	0.014	0.000	0.000	0.000	0.000	0.000	0.020	0.000	0.000
2.220	-1.	10.	0.000	0.100	0.000	0.000	0.000	0.000	0.000	0.000	0.000	0.000
2.220	+0.	10.	0.100	0.000	0.000	0.000	0.000	0.000	0.000	0.000	0.000	0.000
2.250	-1.	10.	0.000	0.067	0.000	0.000	0.000	0.000	0.000	0.000	0.000	0.000
2.250	+0.	10.	0.067	0.000	0.000	0.000	0.000	0.000	0.000	0.000	0.000	0.000
2.600	-1.	12.	0.000	0.050	0.000	0.000	0.000	0.000	0.000	0.000	0.000	0.000
2.600	+0.	12.	0.050	0.000	0.000	0.000	0.000	0.000	0.000	0.000	0.000	0.000
2.700	-1.	14.	0.000	0.033	0.000	0.000	0.000	0.000	0.000	0.000	0.000	0.000
2.700	+0.	14.	0.033	0.000	0.000	0.000	0.000	0.000	0.000	0.000	0.000	0.000
1.232	-2.	4.	0.000	0.995	0.000	0.000	0.000	0.000	0.000	0.000	0.000	0.000
1.232	-1.	4.	0.000	0.332	0.000	0.000	0.000	0.000	0.000	0.000	0.000	0.000
1.232	-0.	4.	0.332	0.000	0.000	0.000	0.000	0.000	0.000	0.000	0.000	0.000
1.232	+1.	4.	0.995	0.000	0.000	0.000	0.000	0.000	0.000	0.000	0.000	0.000
1.600	-2.	4.	0.014	1.204	0.000	0.000	0.000	0.000	0.000	0.000	0.000	0.000
1.600	-1.	4.	0.438	0.834	0.000	0.000	0.000	0.000	0.000	0.000	0.000	0.000
1.600	-0.	4.	0.834	0.438	0.000	0.000	0.000	0.000	0.000	0.000	0.000	0.000
1.600	+1.	4.	1.204	0.014	0.000	0.000	0.000	0.000	0.000	0.000	0.000	0.000
1.620	-2.	2.	0.000	1.077	0.000	0.000	0.000	0.000	0.000	0.000	0.000	0.000
1.620	-1.	2.	0.447	0.806	0.000	0.000	0.000	0.000	0.000	0.000	0.000	0.000
1.620	-0.	2.	0.806	0.447	0.000	0.000	0.000	0.000	0.000	0.000	0.000	0.000
1.620	+1.	2.	1.077	0.000	0.000	0.000	0.000	0.000	0.000	0.000	0.000	0.000
1.700	-2.	4.	0.000	1.057	0.000	0.000	0.000	0.000	0.000	0.000	0.000	0.000
1.700	-1.	4.	0.527	0.880	0.000	0.000	0.000	0.000	0.000	0.000	0.000	0.000
1.700	-0.	4.	0.880	0.527	0.000	0.000	0.000	0.000	0.000	0.000	0.000	0.000
1.700	+1.	4.	1.057	0.000	0.000	0.000	0.000	0.000	0.000	0.000	0.000	0.000
1.750	-2.	2.	0.020	0.545	0.000	0.000	0.000	0.000	0.000	0.000	0.000	0.000
1.750	-1.	2.	0.075	0.250	0.000	0.000	0.000	0.000	0.000	0.000	0.000	0.000
1.750	-0.	2.	0.250	0.075	0.000	0.000	0.000	0.000	0.000	0.000	0.000	0.000
1.750	+1.	2.	0.545	0.020	0.000	0.000	0.000	0.000	0.000	0.000	0.000	0.000
1.900	-2.	2.	0.004	1.059	0.000	0.000	0.000	0.000	0.000	0.000	0.000	0.000
1.900	-1.	2.	0.496	0.847	0.000	0.000	0.000	0.000	0.000	0.000	0.000	0.000
1.900	-0.	2.	0.847	0.496	0.000	0.000	0.000	0.000	0.000	0.000	0.000	0.000
1.900	+1.	2.	1.059	0.004	0.000	0.000	0.000	0.000	0.000	0.000	0.000	0.000
1.905	-2.	6.	0.000	1.026	0.000	0.000	0.000	0.000	0.000	0.000	0.000	0.000
1.905	-1.	6.	0.496	0.924	0.000	0.000	0.000	0.000	0.000	0.000	0.000	0.000
1.905	-0.	6.	0.924	0.496	0.000	0.000	0.000	0.000	0.000	0.000	0.000	0.000
1.905	+1.	6.	1.026	0.000	0.000	0.000	0.000	0.000	0.000	0.000	0.000	0.000
1.910	-2.	2.	0.038	1.347	0.000	0.000	0.000	0.000	0.000	0.000	0.000	0.000
1.910	-1.	2.	0.307	0.744	0.000	0.000	0.000	0.000	0.000	0.000	0.000	0.000
1.910	-0.	2.	0.744	0.307	0.000	0.000	0.000	0.000	0.000	0.000	0.000	0.000
1.910	+1.	2.	1.347	0.038	0.000	0.000	0.000	0.000	0.000	0.000	0.000	0.000
1.920	-2.	4.	0.020	1.260	0.000	0.000	0.000	0.000	0.000	0.000	0.000	0.000
1.920	-1.	4.	0.420	0.833	0.000	0.000	0.000	0.000	0.000	0.000	0.000	0.000
1.920	-0.	4.	0.833	0.420	0.000	0.000	0.000	0.000	0.000	0.000	0.000	0.000
1.920	+1.	4.	1.260	0.020	0.000	0.000	0.000	0.000	0.000	0.000	0.000	0.000
1.930	-2.	6.	0.000	0.150	0.000	0.000	0.000	0.000	0.000	0.000	0.000	0.000
1.930	-1.	6.	0.000	0.050	0.000	0.000	0.000	0.000	0.000	0.000	0.000	0.000
1.930	-0.	6.	0.050	0.000	0.000	0.000	0.000	0.000	0.000	0.000	0.000	0.000
1.930	+1.	6.	0.150	0.000	0.000	0.000	0.000	0.000	0.000	0.000	0.000	0.000
1.940	-2.	4.	0.000	1.061	0.000	0.000	0.000	0.000	0.000	0.000	0.000	0.000
1.940	-1.	4.	0.505	0.858	0.000	0.000	0.000	0.000	0.000	0.000	0.000	0.000
1.940	-0.	4.	0.858	0.505	0.000	0.000	0.000	0.000	0.000	0.000	0.000	0.000
1.940	+1.	4.	1.061	0.000	0.000	0.000	0.000	0.000	0.000	0.000	0.000	0.000
1.950	-2.	8.	0.000	0.839	0.000	0.000	0.000	0.000	0.000	0.000	0.000	0.000

1.950	-1.	8.	0.240	0.519	0.000	0.000	0.000	0.000	0.000	0.000	0.000	0.000
1.950	-0.	8.	0.519	0.240	0.000	0.000	0.000	0.000	0.000	0.000	0.000	0.000
1.950	+1.	8.	0.839	0.000	0.000	0.000	0.000	0.000	0.000	0.000	0.000	0.000
2.000	-2.	6.	0.000	1.097	0.000	0.000	0.000	0.000	0.000	0.000	0.000	0.000
2.000	-1.	6.	0.448	0.965	0.000	0.000	0.000	0.000	0.000	0.000	0.000	0.000
2.000	-0.	6.	0.965	0.448	0.000	0.000	0.000	0.000	0.000	0.000	0.000	0.000
2.000	+1.	6.	1.097	0.000	0.000	0.000	0.000	0.000	0.000	0.000	0.000	0.000
2.150	-2.	2.	0.000	0.100	0.000	0.000	0.000	0.000	0.000	0.000	0.000	0.000
2.150	-1.	2.	0.000	0.033	0.000	0.000	0.000	0.000	0.000	0.000	0.000	0.000
2.150	-0.	2.	0.033	0.000	0.000	0.000	0.000	0.000	0.000	0.000	0.000	0.000
2.150	+1.	2.	0.100	0.000	0.000	0.000	0.000	0.000	0.000	0.000	0.000	0.000
2.200	-2.	8.	0.000	0.070	0.000	0.000	0.000	0.000	0.000	0.000	0.000	0.000
2.200	-1.	8.	0.000	0.023	0.000	0.000	0.000	0.000	0.000	0.000	0.000	0.000
2.200	-0.	8.	0.023	0.000	0.000	0.000	0.000	0.000	0.000	0.000	0.000	0.000
2.200	+1.	8.	0.070	0.000	0.000	0.000	0.000	0.000	0.000	0.000	0.000	0.000
2.300	-2.	10.	0.000	0.050	0.000	0.000	0.000	0.000	0.000	0.000	0.000	0.000
2.300	-1.	10.	0.000	0.017	0.000	0.000	0.000	0.000	0.000	0.000	0.000	0.000
2.300	-0.	10.	0.017	0.000	0.000	0.000	0.000	0.000	0.000	0.000	0.000	0.000
2.300	+1.	10.	0.050	0.000	0.000	0.000	0.000	0.000	0.000	0.000	0.000	0.000
2.350	-2.	6.	0.000	0.050	0.000	0.000	0.000	0.000	0.000	0.000	0.000	0.000
2.350	-1.	6.	0.000	0.017	0.000	0.000	0.000	0.000	0.000	0.000	0.000	0.000
2.350	-0.	6.	0.017	0.000	0.000	0.000	0.000	0.000	0.000	0.000	0.000	0.000
2.350	+1.	6.	0.050	0.000	0.000	0.000	0.000	0.000	0.000	0.000	0.000	0.000
2.390	-2.	8.	0.000	0.080	0.000	0.000	0.000	0.000	0.000	0.000	0.000	0.000
2.390	-1.	8.	0.000	0.027	0.000	0.000	0.000	0.000	0.000	0.000	0.000	0.000
2.390	-0.	8.	0.027	0.000	0.000	0.000	0.000	0.000	0.000	0.000	0.000	0.000
2.390	+1.	8.	0.080	0.000	0.000	0.000	0.000	0.000	0.000	0.000	0.000	0.000
2.400	-2.	10.	0.000	0.070	0.000	0.000	0.000	0.000	0.000	0.000	0.000	0.000
2.400	-1.	10.	0.000	0.023	0.000	0.000	0.000	0.000	0.000	0.000	0.000	0.000
2.400	-0.	10.	0.023	0.000	0.000	0.000	0.000	0.000	0.000	0.000	0.000	0.000
2.400	+1.	10.	0.070	0.000	0.000	0.000	0.000	0.000	0.000	0.000	0.000	0.000
2.420	-2.	12.	0.000	0.100	0.000	0.000	0.000	0.000	0.000	0.000	0.000	0.000
2.420	-1.	12.	0.000	0.033	0.000	0.000	0.000	0.000	0.000	0.000	0.000	0.000
2.420	-0.	12.	0.033	0.000	0.000	0.000	0.000	0.000	0.000	0.000	0.000	0.000
2.420	+1.	12.	0.100	0.000	0.000	0.000	0.000	0.000	0.000	0.000	0.000	0.000
2.750	-2.	14.	0.000	0.050	0.000	0.000	0.000	0.000	0.000	0.000	0.000	0.000
2.750	-1.	14.	0.000	0.017	0.000	0.000	0.000	0.000	0.000	0.000	0.000	0.000
2.750	-0.	14.	0.017	0.000	0.000	0.000	0.000	0.000	0.000	0.000	0.000	0.000
2.750	+1.	14.	0.050	0.000	0.000	0.000	0.000	0.000	0.000	0.000	0.000	0.000
2.950	-2.	16.	0.000	0.040	0.000	0.000	0.000	0.000	0.000	0.000	0.000	0.000
2.950	-1.	16.	0.000	0.013	0.000	0.000	0.000	0.000	0.000	0.000	0.000	0.000
2.950	-0.	16.	0.013	0.000	0.000	0.000	0.000	0.000	0.000	0.000	0.000	0.000
2.950	+1.	16.	0.040	0.000	0.000	0.000	0.000	0.000	0.000	0.000	0.000	0.000
1.116	+0.	2.	0.000	0.000	0.000	0.000	0.000	0.000	0.000	1.000	0.000	0.000
1.405	+0.	2.	0.666	0.494	0.000	0.000	0.000	0.000	0.000	0.000	0.000	0.333
1.520	+0.	4.	0.357	0.281	0.224	0.000	0.000	0.000	0.000	0.092	0.000	0.167
1.600	+0.	2.	0.233	0.173	0.113	0.000	0.000	0.000	0.000	0.000	0.000	0.117
1.670	+0.	2.	0.444	0.372	0.100	0.000	0.000	0.000	0.000	0.382	0.000	0.139
1.690	+0.	4.	0.566	0.481	0.125	0.000	0.000	0.000	0.000	0.250	0.000	0.167
1.800	+0.	2.	0.064	0.060	0.218	0.000	0.000	0.000	0.000	0.009	0.000	0.007
1.810	+0.	2.	0.283	0.249	0.325	0.000	0.000	0.000	0.000	0.000	0.000	0.067
1.820	+0.	6.	0.131	0.110	0.300	0.000	0.000	0.000	0.000	0.081	0.000	0.040
1.830	+0.	6.	0.516	0.417	0.035	0.000	0.000	0.000	0.000	0.206	0.000	0.183
1.890	+0.	4.	0.096	0.082	0.147	0.000	0.000	0.000	0.000	0.053	0.000	0.026
2.020	+0.	8.	0.327	0.250	0.025	0.000	0.000	0.000	0.000	0.030	0.000	0.150
2.100	+0.	8.	0.129	0.120	0.200	0.000	0.000	0.000	0.000	0.050	0.000	0.017
2.110	+0.	6.	0.332	0.288	0.192	0.000	0.000	0.000	0.000	0.056	0.000	0.085
2.325	+0.	4.	0.018	0.018	0.100	0.000	0.000	0.000	0.000	0.020	0.000	0.000
2.350	+0.	10.	0.085	0.068	0.060	0.000	0.000	0.000	0.000	0.020	0.000	0.033
1.189	-1.	2.	0.000	0.483	0.000	0.000	0.000	0.000	0.000	0.000	0.000	0.000
1.193	+0.	2.	0.000	0.000	0.000	0.000	0.000	0.000	0.000	0.000	0.000	1.000
1.197	+1.	2.	0.998	0.000	0.000	0.000	0.000	0.000	0.000	0.000	0.000	0.000
1.383	-1.	4.	0.000	0.967	0.000	0.000	0.000	0.000	0.000	0.880	0.000	0.060
1.384	+0.	4.	0.120	0.089	0.000	0.000	0.000	0.000	0.000	0.880	0.000	0.000

1.387	+1.	4.	1.000	0.000	0.000	0.000	0.000	0.000	0.000	0.880	0.000	0.060
1.660	-1.	2.	0.000	0.133	0.000	0.000	0.000	0.000	0.000	0.070	0.000	0.043
1.660	+0.	2.	0.085	0.063	0.100	0.000	0.000	0.000	0.000	0.070	0.000	0.000
1.660	+1.	2.	0.155	0.000	0.200	0.000	0.000	0.000	0.000	0.070	0.000	0.043
1.670	-1.	4.	0.000	0.434	0.000	0.000	0.000	0.000	0.000	0.100	0.000	0.225
1.670	+0.	4.	0.450	0.334	0.050	0.000	0.000	0.000	0.000	0.100	0.000	0.000
1.670	+1.	4.	0.550	0.000	0.100	0.000	0.000	0.000	0.000	0.100	0.000	0.225
1.750	-1.	2.	0.108	0.439	0.000	0.000	0.000	0.000	0.000	0.114	0.000	0.029
1.750	+0.	2.	0.278	0.265	0.125	0.000	0.000	0.000	0.000	0.114	0.000	0.358
1.750	+1.	2.	0.637	0.105	0.250	0.000	0.000	0.000	0.000	0.100	0.000	0.029
1.775	-1.	6.	0.077	0.559	0.000	0.000	0.000	0.000	0.000	0.276	0.000	0.056
1.775	+0.	6.	0.211	0.184	0.200	0.000	0.000	0.000	0.000	0.276	0.000	0.039
1.775	+1.	6.	0.587	0.061	0.400	0.000	0.000	0.000	0.000	0.276	0.000	0.056
1.915	-1.	6.	0.001	0.316	0.000	0.000	0.000	0.000	0.000	0.098	0.000	0.146
1.915	+0.	6.	0.310	0.235	0.050	0.000	0.000	0.000	0.000	0.098	0.000	0.001
1.915	+1.	6.	0.391	0.001	0.100	0.000	0.000	0.000	0.000	0.098	0.000	0.146
1.940	-1.	4.	0.092	0.711	0.252	0.000	0.000	0.000	0.000	0.107	0.000	0.103
1.940	+0.	4.	0.317	0.267	0.241	0.000	0.000	0.000	0.000	0.107	0.000	0.045
1.940	+1.	4.	0.763	0.072	0.230	0.000	0.000	0.000	0.000	0.107	0.000	0.103
2.030	-1.	8.	0.064	0.730	0.183	0.000	0.000	0.000	0.000	0.332	0.000	0.070
2.030	+0.	8.	0.287	0.252	0.246	0.000	0.000	0.000	0.000	0.332	0.000	0.033
2.030	+1.	8.	0.793	0.050	0.310	0.000	0.000	0.000	0.000	0.332	0.000	0.070
2.070	-1.	6.	0.000	0.111	0.000	0.000	0.000	0.000	0.000	0.000	0.000	0.075
2.070	+0.	6.	0.150	0.111	0.040	0.000	0.000	0.000	0.000	0.000	0.000	0.000
2.070	+1.	6.	0.150	0.000	0.080	0.000	0.000	0.000	0.000	0.000	0.000	0.075
1.315	+0.	2.	0.000	0.000	0.000	0.000	0.000	0.000	0.000	0.000	0.000	0.000
1.321	+1.	2.	0.000	0.000	0.000	0.000	0.000	0.000	0.000	0.000	0.000	0.000
1.532	+0.	4.	0.000	0.667	0.000	0.000	0.000	0.000	0.000	0.000	0.000	0.000
1.535	+1.	4.	0.667	0.000	0.000	0.000	0.000	0.000	0.000	0.000	0.000	0.000
1.823	+0.	4.	0.111	0.222	0.000	0.000	0.000	0.000	0.000	0.500	0.000	0.000
1.823	+1.	4.	0.222	0.111	0.500	0.000	0.000	0.000	0.000	0.500	0.000	0.000
2.025	+0.	6.	0.000	0.258	0.533	0.000	0.000	0.000	0.000	0.200	0.000	0.267
2.025	+1.	6.	0.258	0.000	0.267	0.000	0.000	0.000	0.000	0.200	0.000	0.267
1.672	+1.	4.	0.236	0.000	0.678	0.000	0.000	0.000	0.000	0.678	0.000	0.000

Bibliography

[1] T. Lee and G. Wick, Phys. Rev. D9 (1974) 2991.

[2] T. Akesson et al., Nucl. Phys. B353 (1991) 286.

[3] I. Tserruya, CERN-PPE/95-185.

[4] J. Rafelski, Phys. Rep. 88 (1982) 331.

[5] K. Werner, Phys. Rep. 232 (1993) 87.

[6] T. Alber et al., Phys. Rev. Lett. 75 (1995) 3814.

[7] J. Bjorken, Phys. Rev. D27 (1983) 140.

[8] P. Braun-Munziger, J. Stachel, J. P. Wessels and N. Xu, SUNY-RHI-95-85.

[9] B. Müller, Lecture Notes in Physics 225: The Physics of the Quark-Gluon Plasma, Springer-Verlag (1985) 25.

[10] D. Di Bari et al., Nucl. Phys. A590 (1995) 307c; J. Kinson et al.,Nucl. Phys. A590 (1995) 317c.

[11] T. Matsui and H. Satz, Phys. Lett. B178 (1986) 416.

[12] S. Ramos et al., Nucl. Phys. A590 (1995) 117c.

[13] G. Agakichiev et al., Phys. Rev. Lett. 75 (1995) 1272.

[14] E. Shuryak, Phys. Lett. B78 (1978) 150.

[15] F. Cooper and G. Frye, Phys. Rev. D10 (1974) 186.

[16] G. Odyniec, in *Hot Hadronic Matter: Theory and Experiment*, J. Letessier, H. Gutbrod ands J. Rafelski (Eds.), Plenum Press, New York (1995) 405.

[17] E. Schnedermann, J. Sollfrank and U. Heinz, Phys. Rev. C48 (1993) 2462.

[18] S. Weinig, Ph.D. thesis, Universität Frankfurt (1990); NA35 Coll. J. Bartke et al., Z. Phys. C48 (1990) 191.

[19] E802 Coll., P. Vincent, M. Sarabura, H. Hamagaki et al., Nucl. Phys. A498 (1989) 67c, 409c, 415c; T.Abbott et al Phys. Rev. Lett. 64 (1990) 847.

[20] J. Cleymans, H. Satz, E. Suhonen and D. von Oertzen in *Proceedings: Phase structure of strongly interacting matter*, J. Cleymans (Ed)., Springer-Verlag, (1990) 266.

[21] Yu.M. Sinyukov, V. Averchenkov and B. Lörstadt, Z. Phys. C49 (1991) 417; M. Kataja, Z. Phys. C38 (1988) 419.

[22] P. Siemens and J. Rasmussen, Phys. Rev. Lett. 42 (1979) 880.

[23] E. Schnedermann and U. Heinz, Phys. Rev. Lett. 69 (1992) 2908.

[24] J. Barrette et al., E877 Coll., Phys. Rev. Lett. 73 (1994) 2352.

[25] N. Bilić, J. Cleymans, K. Redlich and D. Srivastava, private communication.

[26] J. Cleymans and H. Satz, Z. Phys. C57 (1993) 135.

[27] J. Cleymans, K. Redlich, H. Satz and E. Suhonen, Z. Phys. C58 (1993) 347.

[28] U. Heinz, Nucl. Phys. A566 (1994) 225c.

[29] P. Braun-Munziger, J. Stachel, J. P. Wessels and N. Xu, Phys. Lett. B344 (1995) 43.

[30] P. Braun-Munziger and J. Stachel, in *Hot Hadronic Matter: Theory and Experiment*, J. Letessier, H. Gutbrod ands J. Rafelski (Eds.), Plenum Press, New York (1995) 451.

[31] M. Gorenstein, H. Miller, R. Quick and S. Yang, Phys. Rev. C50 (1994) 2232.

[32] J. Letessier, A. Tounsi, U. Heinz. J. Sollfrank and J. Rafelski, Phys. Rev. D51 (1995) 3408.

[33] P.Braun-Munzinger, J.Stachel et al., Phys. Lett. B216 (1989) 1.

[34] *Review of Particle Properties* Phys. Rev. D50 (1994) 1177.

[35] D. Hill and J. Wheeler, Phys. Rev. 89 (1953) 1124.

[36] Y. Wang, Nucl. Phys. A566 (1994) 379c;
Y. Wang, in *Heavy Ion Physics at the AGS*, G. S. F. Stephans et al. (Eds.), MITLNS-2158, (1993) 239.

[37] G. Odyniec, in *Hot Hadronic Matter: Theory and Experiment*, J. Letessier, H. Gutbrod ands J. Rafelski (Eds.), Plenum Press, New York (1995) 402.

[38] W. A. Zajc, Nucl. Phys. A544 (1992) 237c;
M. Gonin, in *Heavy Ion Physics at the AGS*, G. S. F. Stephans et al. (Eds), MITLNS-2158, (1993) 184.

[39] G. Odyniec, in *Hot Hadronic Matter: Theory and Experiment*, J. Letessier, H. Gutbrod ands J. Rafelski (Eds.), Plenum Press, New York (1995) 399.

[40] G.S.F. Stephans, Nucl. Phys. A566 (1994) 269c.

[41] M. Gazdzicki and D. Röhrich, Z. Phys. C65 (1995) 215.

[42] J. Stachel, private communication to J. Cleymans.

[43] B. Shiva Kumar, in *Heavy Ion Physics at the AGS*, G. S. F. Stephans et al. (Eds.), MITLNS-2158, (1993) 144.

[44] M. Gazdzicki, private communication to J. Cleymans.

[45] A. O. Vaisenberg et al., JETP Lett. 29 (1979) 661.

[46] B. Z. Kopeliovich and F. Niedermayer, Phys. Lett. B 151 (1985) 437.

[47] S. Kahana et al., Phys. Rev. C47 (1993) 1356.

[48] J. Cleymans, H. Satz, E. Suhonen and D. von Oertzen, Phys. Lett. B242, (1990) 111; N. Davidson, H. Miller, R. Quick, and J. Cleymans, Phys. Lett. B255, (1991) 105; N. Davidson, H. Miller and D. von Oertzen, Phys. Lett. B256 (1991) 554.

[49] J. Letessier, J. Rafelski and A. Tounsi, Phys. Lett. B328 (1994) 499.

[50] T. K. Hemmick et al., Nucl. Phys. A566 (1994) 431c.

[51] D. Rischke, M. Gorenstein, H. Stocker and W. Greiner, Z. Phys. C51 (1991) 485; J. Cleymans, M. Gorenstein, J. Stalnacke and E. Suhonen, Phys. Scripta 48 (1993) 485.

[52] U. Heinz, P. Koch, K. Lee, E. Schnedermann and H. Weigert in *Proceedings: Phase structure of strongly interacting matter*, J. Cleymans (Ed.), Springer-Verlag (1990) 104.

[53] J. Cleymans, D. Elliott, H. Satz and R. Thews, *Proceedings: International Conference on Nuclear Physics at the Turn of the Millennium: Structure of Vacuum and Elementary Matter*, Wilderness, South Africa (1996) to be published.

[54] A. Panagiotou, G. Mavromanolakis and J. Tzoulis, UA/NPPD-1-95 (1995).

[55] J. Rafelski, Nucl. Phys. A544 (1992) 279c.

[56] A. Panagiotou, G. Mavromanolakis and J. Tzoulis, in paper entitled *"Negative strange quarkchemical potential. Indication of phase transition to deconfined quark matter. First possible experimental evidence"* submitted (1996) to Phys. Rev. C for refereeing.

[57] M. Gorenstein and S. Yang, Phys. Rev. C44 (1991) 2875.

[58] D. Rischke, M. Gorenstein, H. Stöcker and W. Greiner Z. Phys. C51 (1991) 485.

[59] J. Cleymans, M. Gorenstein, J. Stalnacke and E. Suhonen, Phys. Scr. 48 (1993) 277.

[60] M. Gonin, Nucl. Phys. A553 (1993) 799c.

[61] A. Prudnikov, U. Brischkov and O. Maritsev, *Integrals and Series: Special Functions*, Moscow (1983) 378.

Acknowledgements

I would like to thank my supervisor Prof. Jean Cleymans for his knowledge, enthusiasm and approachability during this degree. It has been inspirational working with him and enjoying Physics with lots of laughs.
Prof. Cleymans had an array of distinguished collaborators and visitors during this time, all of whom contributed to my appreciation of this field of Physics. They were: Professors H. Satz, R. Thews, A. Panagiotou, M. Gorenstein, M. Chaichian, B. Müller, L. McLerran, D. Srivastava and K. Redlich. A special thanks to Dr. Neven Bilić for the 'personalised' Quantum Field Theory course, and his allround assistance. Thanks too to Prof. Cleyman's secretary, Joan Parsons, for all her assistance and shared love of sport.

The Foundation for Research and Development (FRD) contributed substantially to this degree. I am truly grateful, and hope I shall continue to receive some of this generous support for further study.

Thanks to my wonderful mother and her husband, Fred, who supplied me with desks and motorcars and food in my hours of need.

Thanks to Kevin and Michele Smith for the fine routes, and Mark and Mereté and the 'biscuits' of Merced.

A special thanks to Mt. Robson for allowing me to complete this degree.

Thanks also to Messers G. Puccini, W. Mozart, D. Maradona, C. Lewis, J. Hendrix, A. Senna, F. Fellini, R. Zimmerman and J. Daniels. Deep thanks to Led Zeppelin and the one who so recently left us, yet stopped long enough to show me 'the Golden Road to Unlimited Devotion'.